

## Article

# Zircons from Collisional Granites, Garhwal Himalaya, NW India: U–Th–Pb Age, Geochemistry and Protolith Constraints

Sumit Mishra <sup>1,\*</sup> , Alexander I. Slabunov <sup>2,\*</sup>, Sergei A. Svetov <sup>2</sup> , Anna V. Kervinen <sup>2</sup> and Natalia S. Nesterova <sup>2</sup>

<sup>1</sup> Department of Geology, School of Earth Sciences, H.N.B. Garhwal University, Garhwal, Srinagar 246174, Uttarakhand, India

<sup>2</sup> Karelian Research Centre RAS, Institute of Geology, 185910 Petrozavodsk, Russia; doc\_svs@mail.ru (S.A.S.); kervinen@mail.ru (A.V.K.); nest345@gmail.com (N.S.N.)

\* Correspondence: smpsgeo@gmail.com (S.M.); slabunov@krc.karelia.ru (A.I.S.)

**Abstract:** In the present work, we studied zircons from the less foliated granites of the Chail Group, which form a thrust sheet of the Lesser Himalayan Sequences, Garhwal region. Compositionally, these granites are S-type, formed in a collisional tectonic setting. Zircons possess an internal structure, mineral inclusions, and geochemical characteristics typical of magmatic origin. The U–Th–Pb geochronology and geochemistry were assessed using the laser ablation multi-collector inductively coupled plasma spectrometry (LA–ICP–MS) technique. U–Th–Pb isotope dating of zircons from two different samples revealed their age, estimated from the upper intersection of the discordia, to be  $1845 \pm 19$  Ma. Zircons from one sample contained inherited cores belonging to three age groups: Paleoproterozoic (3.52 Ga), Neoproterozoic (2.78 Ga and 2.62 Ga), and Paleoproterozoic (2.1 Ga). Zircons with ages of 3.52, 2.62, and 2.1 Ga were interpreted as magmatic based on their geochemical characteristics. The 2.78 Ga core was interpreted as metamorphic. The observed inheritance is consistent with the melting of sedimentary rocks. The inherited zircons could have originated from Aravalli and Bundelkhand Craton and Paleoproterozoic Aravalli Fold Belt rocks. This confirms that the studied granites are S-type and could have been formed in a collisional environment at 1.85 Ga on the western flank of the Columbia Supercontinent.

**Keywords:** zircon; Lesser Himalayas; granites; Paleoproterozoic; U–Th–Pb age; Himalayas



**Citation:** Mishra, S.; Slabunov, A.I.; Svetov, S.A.; Kervinen, A.V.; Nesterova, N.S. Zircons from Collisional Granites, Garhwal Himalaya, NW India: U–Th–Pb Age, Geochemistry and Protolith Constraints. *Minerals* **2021**, *11*, 1071. <https://doi.org/10.3390/min11101071>

Academic Editor: Annamaria Fornelli

Received: 29 July 2021

Accepted: 23 September 2021

Published: 29 September 2021

**Publisher's Note:** MDPI stays neutral with regard to jurisdictional claims in published maps and institutional affiliations.



**Copyright:** © 2021 by the authors. Licensee MDPI, Basel, Switzerland. This article is an open access article distributed under the terms and conditions of the Creative Commons Attribution (CC BY) license (<https://creativecommons.org/licenses/by/4.0/>).

## 1. Introduction

Zircon ( $\text{ZrSiO}_4$ ) is an accessory mineral constituent of the majority of igneous and metamorphic rocks, with the zirconium element (Zr) serving as a structural constituent [1]. Trace elements (e.g., U, Th, Hf, Y and Lanthanide–rare earth elements (REEs)) are present in zircons in significant amounts [2–4]. Zircon resists alteration in a wide variety of geological settings. The isotopic ratios of the elements within the zircons provide ages and parent magma constraints because of their early formation and refractory nature during subsequent events [1,5–7]. The U–Pb ages determined from zircons have traditionally been considered the most accurate method for determining the meaningful crystallization age of granitoids. Additionally, zircon geochemistry can provide valuable information to establish the conditions of the environment under which the granitoids were emplaced.

The use of zircons as geochronometers is significant when geological criteria for rock dating are hard to determine due to the architectural characteristics of the study area. For example, Himalayan and other collisional orogens are collages of thrust sheets (Figure 1), where most contacts are tectonic and create difficulties in estimating the relative ages of geological bodies. In Lesser Himalayan Sequences (LHS), the thrust sheets comprising variably deformed and low-to-medium-grade metamorphosed igneous and sedimentary rocks lack distinctive field characteristics. Dating of the rocks within the thrust sheets and the correlation of ages and inherited age patterns to other tectonic units may help to characterize these sheets.

Geochronological data derived from Himalayan granitoids reveal their emplacement, cooling, and exhumation history [8]. These data show distinct periods of magmatic activity around 2100–1800, 1200–1000, 600–400, 100–50, and 25–15 Ma in the region [9]. Various geochemical, geochronological, and isotopic data have been used extensively in previous research on the Himalayas, indicating that granitic magmas formed during rifting, subduction, or accretion events [10–13]. The zircon U–Th–Pb ages of Lesser Himalayan granites range from around 2200 to 1750 Ma, and their age pattern resembles the ages obtained from the Columbia Supercontinent in the Paleoproterozoic time [14].

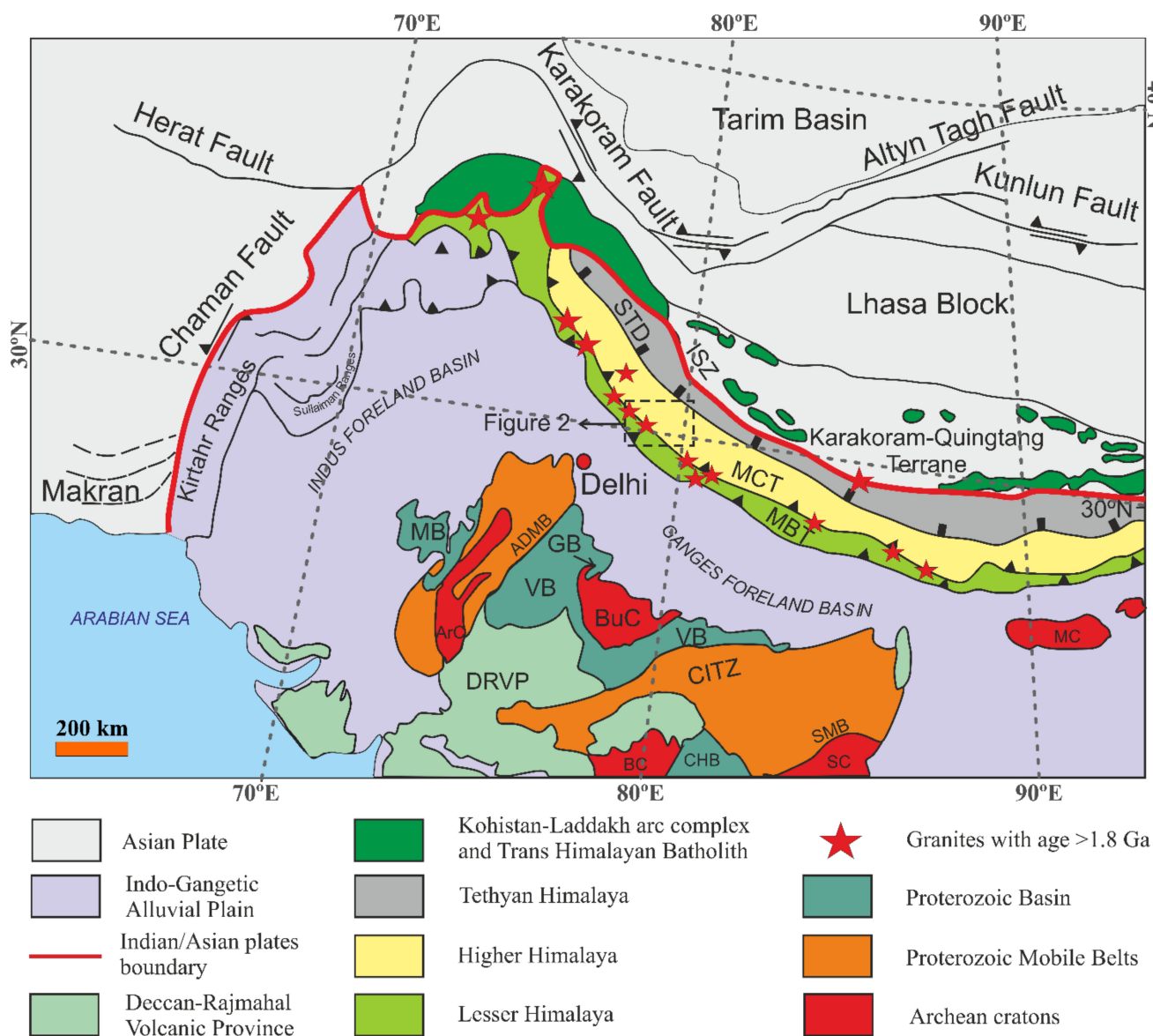


**Figure 1.** Simplified geological and tectonics map of the northernmost part of India and surrounding boundary zone of the Indian subcontinent, showing the principal components of the Indian Shield [15]. (Abbreviations: ArC: Aravalli Craton; BuC: Bundelkhand Craton; BC: Bastar Craton; SC: Singhbhum Craton; MB: Meghalaya Craton; GB: Gwalior basin; VB: Vindhyan basin; MB: Marwar basin; CHB: Chhattisgarh basin; CITZ: Central Indian tectonic zone; MB: Marwar basin; ADMB: Aravalli–Delhi mobile belt; SMB: Singhbhum mobile belt; MBT: Main boundary thrust; MCT: Main central thrust; STD: South Tibetan detachment; ISZ: Indus suture zone; DRVP: Deccan–Rajmahal Volcanic Province).

This paper analyzes the morphological and geochemical characteristics and isotopic ages of zircons from Precambrian Lesser Himalayan granites. It determines their possi-

ble protolith based on analytical results. To date, no U–Th–Pb ages of zircons or their geochemistry have been determined for the study area.

## 2. Geological Background

Four major tectonic zones are identified laterally from south to north in the Himalayan belt, with a length of more than 2400 km: (1) Sub-Himalaya, (2) Lesser Himalayan Sequences, (3) Higher Himalayan Crystalline, and (4) Tethyan Himalaya (Figure 1, [15–17]). The Sub-Himalaya thrusts over the Indo-Gangetic plane along the Main Frontal Thrust (MFT), comprising Miocene to Pleistocene molasses and sediments derived from Himalaya [18]. The Lesser Himalayan Sequences consist of Paleoproterozoic to Early Mesoproterozoic rocks unconformably overlain by Early Cambrian, Upper Paleozoic to Cenozoic rocks and thrust over the Sub-Himalaya along the Main Boundary Thrust (MBT) [19]. The north-dipping Main Central Thrust (MCT) is one of the essential tectonic structures in the Himalayas. It is recognized as an intra-continental shear zone associated with isograde inverted metamorphism [20]. MCT separates Lesser Himalayan Sequences from Higher Himalayan Crystallines. Higher Himalayan Crystallines comprise medium- to high-grade metamorphic sequences ranging from greenschist to upper amphibolite facies [21] and are intruded by granites of Ordovician (c. 485–440 Ma) and early Miocene (c. 22 Ma) age.

The study area comprises the Chail/Ramgarh thrust sheets of Lesser Himalayan Sequences (LHS) in the Garhwal region [22], considered an eastward extension of the Ramgarh Group [23,24]. The Chail Group is a nappe overlaying the poorly metamorphosed LHS, constrained by the Jutogh and Chail Thrusts [21]. Jutogh–Almora and Chail/Ramgarh have been identified as low-to-medium-grade metasedimentary thrust sheets in LHS [18] (Figure 2). Paleoproterozoic granite gneiss and granite augen gneiss are an integral component of LHS. These Paleoproterozoic rocks in the Chail/Ramgarh Group occur as less foliated granites and gneisses with augen gneisses [24,25]. The Chail/Ramgarh Group comprises a package of low-grade metamorphic rocks, including phyllites, phyllitic quartzite, psammitic schists, orthoquartzites, chlorite schist limestones, and meta-basics [26].

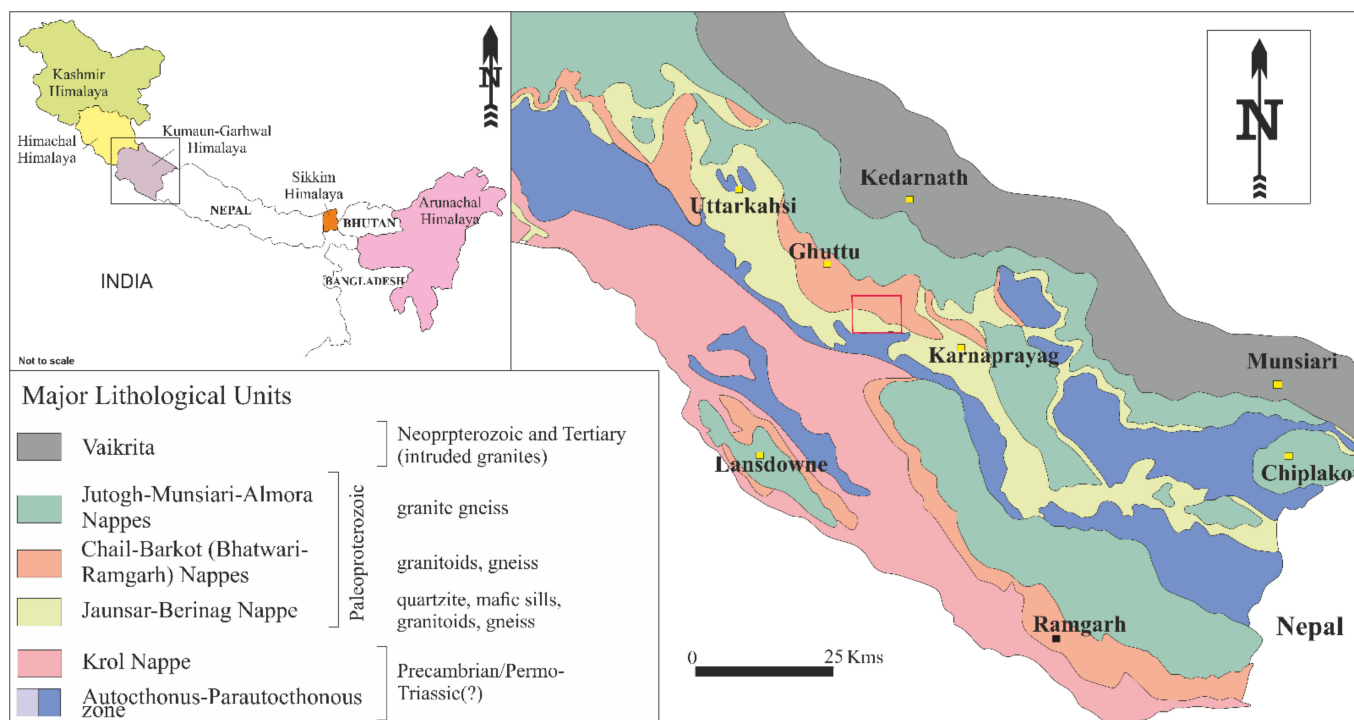
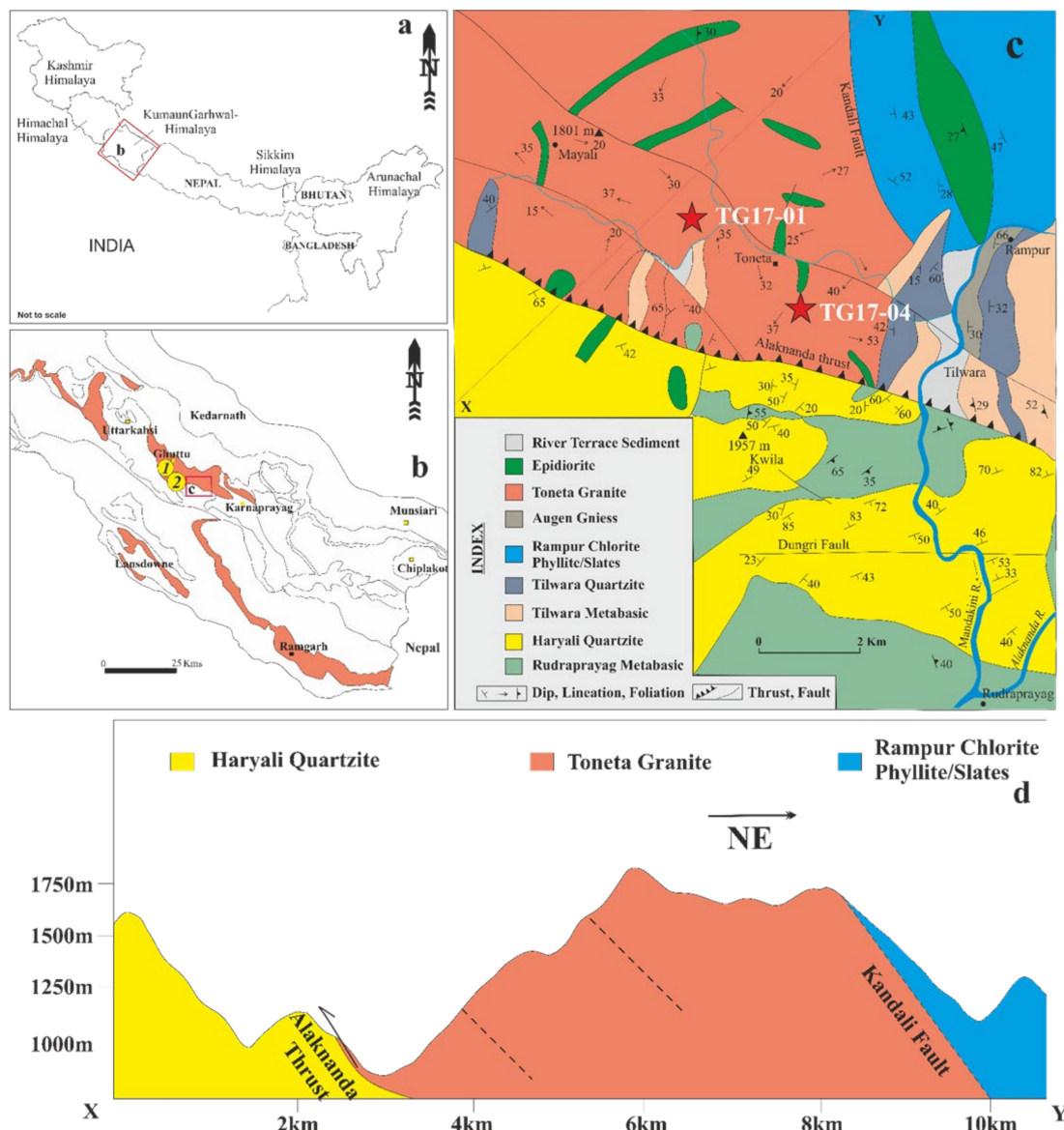


Figure 2. Simplified geological map of Kumaun–Garhwal Himalaya [22].

Rb–Sr isochron ages for granite bodies adjacent to the study area (Chirbatiya Khal granites) are dated  $1768 \pm 131$  Ma (4 points) with an initial  $^{86}\text{Sr}/^{87}\text{Sr}$  ratio of  $0.732 \pm 0.147$  [27]. Rb–Sr dating for granites exposed in the Ghuttu area (Chailli granites) gave an isochron age of  $2120 \pm 60$  Ma, with an initial ratio of  $0.710 \pm 0.020$  interpreted as the age of emplacement for these granites [28]. These ages are potentially imprecise using only the Rb–Sr isochron technique, which can give misleading ages due to the complications of recrystallization in old and deformed rocks; however, the initial ratios are likely relatively accurate. They suggest a source of old and/or radiogenic material.

### 3. Sampling and Petrographic Characteristics

Two granite samples, TG17-01 (N  $30^{\circ}21'27''$ , E  $78^{\circ}57'32''$ ) and TG17-04 (N  $30^{\circ}21'28''$ , E  $78^{\circ}57'13''$ ), which were less foliated, collected for the present study, are shown in Figure 3.



**Figure 3.** Location map of the study area. (a) Northern part of India and (b) location marked in inset map of Uttarakhand (Tropical pink: granite; yellow circle 1: Chailli granite,  $2120 \pm 60$  Ma, and yellow circle 2: Chirbatiya Khal granite,  $1768 \pm 131$  Ma); (c) Geological map of the study area (modified after [23] with sample locations); (d) Geological cross-section sketch.

The granites are well-exposed around Toneta village, situated on the Tilwara–Mayali State Highway (Figure 3). At some places in the Toneta village area, the granites are foliated and show gneissose structures. Both samples, TG17-01 (Figure 4a,b) and TG17-04 (Figure 4c,d), are coarse-grained and less foliated, containing quartz and feldspar megacrysts with biotite and muscovite minerals. In relatively undeformed granite, where a porphyritic texture is clear, muscovite is apparently primary, making it likely that the protolith is peraluminous (contains muscovite  $\pm$  biotite and no primary amphibole). These two mica granites have an accessory phase assemblage of zircon, apatite, minor tourmaline, and minor garnet in our two samples. The garnet is strongly associated with muscovite in foliated planes. Most of the minerals observed under the microscope are subhedral, although euhedral mineral grains are also present in the rocks (Figure 5a). Mica minerals follow the foliation direction. Muscovite has a parallel extension and second-order color under cross-polarized light (Figure 5b). Millimeter subhedral garnet grains have also been observed in some thin sections.



**Figure 4.** (a) Toneta granite exposed 4 km from the road in Tilwara towards Mayali; (b) close-up view of Sample TG17-01 showing porphyritic texture; (c) massive exposure of Toneta granite along with Tilwara–Mayali State Highway (Sample TG17-04); (d) close-up view of Sample TG17-04.

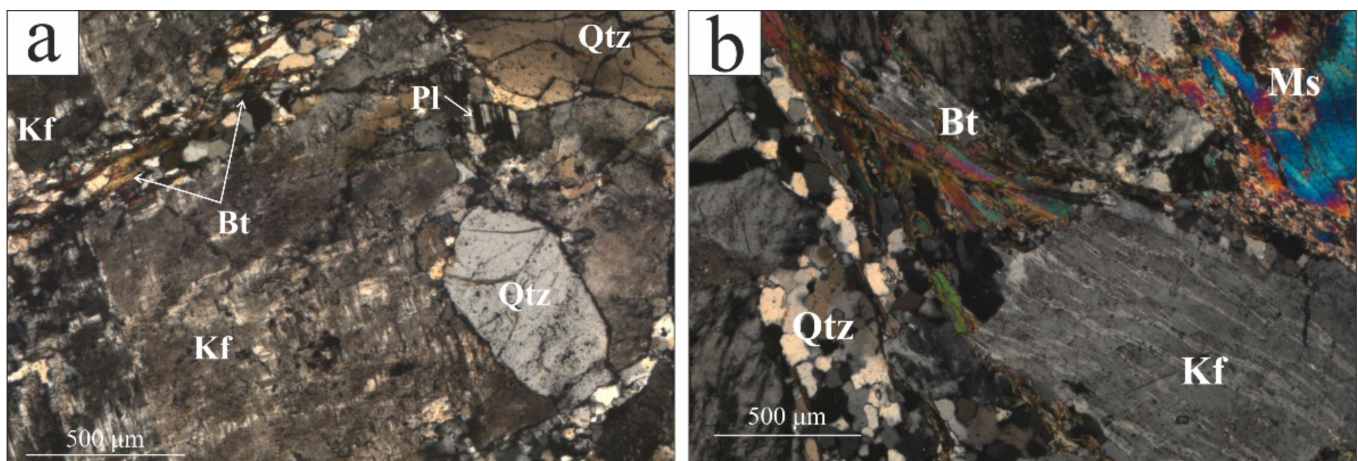


**Figure 5.** Photomicrograph of the thin section (in XPL) studied granite samples: (a) Sample TG17-01; (b) Sample TG17-04. (Mineral symbols taken from [29]).

#### *S-Type Characteristics of Granites*

The studied granite, TG17-01 and TG17-04 (Table S1), in whole-rock geochemical analysis (detailed methodology described in Appendix A), has  $\text{SiO}_2$ , 73.42 and 75.34 (wt. %);  $\text{Al}_2\text{O}_3$ , 13.26 and 12.76 (wt. %);  $\text{Na}_2\text{O}$ , 1.06 and 2.47 (wt. %);  $\text{K}_2\text{O}$ , 6.25 and 4.82 (wt. %); and  $\text{P}_2\text{O}_5$ , 0.23 and 0.2 (wt. %) (Table S1). The samples have normative corundum (4.617 and 3.431), and A/CNK values, 1.44 and 1.30, underline their strongly peraluminous nature. In the ACF ( $\text{Al}_2\text{O}_3$ –CaO–(FeO + MgO)) diagram in [30] and the  $\text{K}_2\text{O}$  versus  $\text{Na}_2\text{O}$  diagram [31], samples are falls in an S-type granite field (Figure S1a,b). The low  $\text{P}_2\text{O}_5$  content and its negative correlation with  $\text{SiO}_2$  suggest that the granites have S-type affinity (Figure S1c). Moreover, in  $\text{SiO}_2$  versus  $\text{K}_2\text{O} + \text{Na}_2\text{O} - \text{CaO}$  diagrams [32], both samples are plotted in an S-type granite field (Figure S1d). In a source discrimination diagram [33], the sample plot in the meta-sediments field indicates that the granitic magma is the product of the partial melting of metasedimentary rocks (Figure S2). The trace elements Ba, Sr, Nb, and Ti, are low, and Rb, Th, U, and Pb are high in the samples [34] (Figure S3), typical for S-type granites and interpreted as syn-collision on the discrimination diagram after [35] (Figure S4).

#### **4. Analytical Methods**

##### *Zircon U–Th–Pb Geochronology*

Zircon separation was performed at the Wadia Institute of Himalayan Geology (WIHG), Dehradun, India, with the procedure outlined in the following [36,37]. A quantity of 4–5 kg of granite from each sample was crushed using a jaw crusher and a disk mill. To concentrate heavy minerals in the samples, magnetic, gravitational, and electrical methods were used. Heavy liquid (bromoforn) was used to separate zircons and other heavy minerals. The zircons were hand-picked under a binocular microscope. Epoxy resin was used to mount the zircons. We polished the zircons in order to expose their surfaces. To investigate their internal structure, they were then examined under optical, back-scatter electron (BSE), and cathodoluminescence (CL) microscopes. The mineral structure and inclusion chemistry of the zircon and BSE images were obtained with an acceleration voltage of 15 kV, a beam current of  $15 \pm 0.05$  nA, and a counting time of 10–15 s using a Vega II LSH (TESCAN, Brno, Czech Republic) scanning electron microscope (SEM) equipped with an energy-dispersive microanalyzer (INCA Energy 350 from the Institute of Geology of the Karelian Research Center, RAS, Petrozavodsk, Russia).

In situ analyses of U–Th–Pb isotopes and trace elements of zircons were performed using ICP–MS Agilent 7500 Ce with a Complex Pro102 (LA–ICP–MS) laser ablation system with a  $\sim 30$   $\mu\text{m}$  spot diameter at Peking University, China. Helium was used to enhance the transport efficiency, and nitrogen was added to the argon plasma to lower the detection

limit and improve analytical precision. Each spot incorporated a background acquisition of approximately 15 s (gas blank), followed by 30 s of sample data acquisition. The laser output fluence was constant and set to 6.0 J/cm<sup>2</sup>. The offline selection and integration of analytical and background signals, correction for time drift, and quantitative calibration for trace element analysis and U–Pb dating were performed with ICPMSDataCal and Glitter 4.0 software (CSIRO). Its algorithm is based on the creation of a three-dimensional diagram in coordinates <sup>206</sup>Pb/<sup>238</sup>U, <sup>207</sup>Pb/<sup>235</sup>U, and <sup>208</sup>Pb/<sup>232</sup>Th; it includes the solution of a system of the equations connecting the maintenance of radiogenic and general Pb, the maintenance of modern non-radiogenic Pb, and the age and quantity of the lost Pb [38]. The zircon 91500 [39] was used as the primary reference material and Plesovice [40] as the secondary. The average value of age during the analytical session for the Plesovice (the accepted age—337.13 ± 0.37 Ma [40]) was 347 ± 15 Ma, and for 91500 (the accepted age—1062.4 ± 0.4 Ma [39]), it was 1071 ± 35 Ma. Common Pb correction was performed using the LAM-ICPMS Common Lead Correction calibration algorithm [41]. Data processing was carried out using the SQUID and Isoplot 4 programs [42]. Analytical errors for individual analyses are given with one-sigma uncertainty. In contrast, the mean ages for the pooled analyses are quoted with two-sigma uncertainty. The reference materials used in the analysis for trace elements were NIST SRM 610, 612, 614 (Standard Reference Material of the National Institute of Standards and Technology, USA) [43]. They were used as samples for calibration, quality control (Table S2), and inter-laboratory comparisons of concentration trace elements.

## 5. Zircon Morphology, Geochemistry, and Age

### 5.1. Zircon Morphology

The zircon crystals in Sample TG17-01 are transparent, pale yellowish–brownish, or colorless (clear) (uncommon). The degree of fracturing varies from almost going unnoticed at the grain margins to becoming highly longitudinal–transverse over the entire grain surface. Larger fractures are often filled with quartz. The crystals fall into two morphological types: sub-idiomorphic prismatic crystals with an elongation coefficient of 1.5–2.5 (approximately 90% of the samples) predominate; isometric grains, typically with many small, irregular facets, are less common. The prismatic crystals display sharp and obtuse dipyrramids, whereas, in more elongated crystals, sharp dipyrramids are not well-shaped. The common occurrence of asymmetrical crystals indicates zircon crystallization in the presence of the closely spaced grains of other minerals. Crystals with a prismatic habit typically exhibit slightly rounded facets. Their grains are 100–210 µm in size. Their internal structure in CL and BSE images is homogeneous for most zircons (no inclusions), except for one grain. The grain with spot T01-9 (Table 1) is dark in CL, with many micro-veins. It is only one of the examples of a metamictic zircon. Some of the grains show slight zoning near their tips (Figure 6a). There is a variety of included mineral phases. They are micron-sized (10–20 µm) quartz, apatite, thorite, biotite, and allanite inclusions that occur in the central portions of zircon grains. In contrast, intergrowths with monazite, up to 30 µm in size, are encountered at the margins.

**Table 1.** U–Th–Pb isotope (LA–ICP–MS) data for zircons from Lesser Garhwal Himalaya (India) granite (TG17-01 and TG17-04).

Sample	Concentrations (ppm)			Isotopic Ratios					Isotopic Age (Ma)						D				
Spot	Th, ppm	U, ppm	Th/U	<sup>207</sup> Pb/ <sup>235</sup> U	1s	<sup>206</sup> Pb/ <sup>238</sup> U	1s	Rho	<sup>208</sup> Pb/ <sup>232</sup> Th	1s	<sup>207</sup> Pb/ <sup>206</sup> Pb	1s	<sup>206</sup> Pb/ <sup>238</sup> U	1s	<sup>207</sup> Pb/ <sup>235</sup> U	1s	<sup>208</sup> Pb/ <sup>232</sup> Th	1s	(%)
TG17-01																			
T01-1	202.4	838.45	0.241	2.80549	0.08363	0.19528	0.00207	0.88	0.05678	0.00056	1700	60	1150	11	1357	22	1116	11	48
T01-2	383.04	681.17	0.562	3.97339	0.09458	0.24858	0.00238	0.9	0.06042	0.00124	1894	29	1431	12	1629	19	1186	24	32
T01-3	120.73	797.12	0.151	4.39939	0.10315	0.28408	0.00268	0.9	0.08521	0.00188	1837	29	1612	13	1712	19	1653	35	14
T01-4	104.44	722.92	0.144	4.18327	0.0993	0.27225	0.00259	0.9	0.08124	0.00184	1823	29	1552	13	1671	19	1579	34	17
T01-5	175.63	1357.78	0.129	2.25813	0.05448	0.14741	0.00139	0.89	0.04258	0.00036	1817	48	886	8	1199	17	843	7	105
T01-6	157.77	3641.7	0.043	0.73266	0.05671	0.05953	0.00069	0.86	0.01759	0.00547	1410	155	373	4	558	33	352	109	278
T01-7	162.52	3804.51	0.043	0.27246	0.03161	0.02718	0.00035	0.87	0.00821	0.00322	1006	248	173	2	245	25	165	65	482
T01-8	310.83	3408.13	0.091	0.36982	0.0217	0.02923	0.00034	0.85	0.00861	0.00079	1462	117	186	2	320	16	173	16	686
T01-9	263.88	3387.32	0.078	0.28249	0.02063	0.0224	0.00027	0.86	0.0066	0.00098	1456	145	143	2	253	16	133	20	918
G01-1	248.13	751.03	0.330	3.31733	0.07487	0.21288	0.00199	0.9	0.06159	0.00136	1847	27	1244	11	1485	18	1208	26	48
G01-2	2541.15	10,384.29	0.245	0.04924	0.00339	0.00775	0.00007	0.58	0.00286	0.00042		153	49.8	0.5	49	3	58	8	-
G01-3	105.99	615.77	0.172	4.79192	0.10505	0.31321	0.00281	0.89	0.09049	0.00073	1815	44	1756	14	1783	18	1751	13	3
G01-4	529.33	1357.52	0.390	2.03342	0.0513	0.13515	0.00125	0.89	0.03911	0.00032	1785	50	817	7	1127	17	775	6	118
G01-5	256.6	1005.08	0.255	2.50073	0.06122	0.17226	0.00153	0.88	0.05004	0.00044	1719	49	1025	8	1272	18	987	8	68
G01-6	343.1	1193.91	0.287	2.13105	0.04941	0.13829	0.00131	0.9	0.02472	0.00063	1827	28	835	7	1159	16	494	12	119
G01-7	98.37	911.71	0.108	3.02769	0.07003	0.19752	0.00177	0.88	0.05706	0.0007	1819	46	1162	10	1415	18	1122	13	57
G01-8	88.58	1025.67	0.086	2.57907	0.06157	0.16824	0.00162	0.88	0.0486	0.00044	1819	48	1002	9	1295	17	959	9	82
G01-9	204.8	535.92	0.382	4.73559	0.11179	0.30424	0.00297	0.9	0.08472	0.00193	1845	29	1712	15	1774	20	1644	36	8
G01-10	595.86	734.03	0.812	3.17851	0.07083	0.20648	0.0019	0.9	0.04614	0.00092	1825	27	1210	10	1452	17	912	18	51
G01-11	149.69	757.25	0.198	3.5619	0.08043	0.23455	0.00213	0.89	0.06782	0.00055	1802	45	1358	11	1541	18	1326	10	33
G01-12	176.21	1836.2	0.096	1.2389	0.02925	0.08328	0.00075	0.88	0.02413	0.00028	1764	47	516	4	818	13	482	5	242
G01-13	216.59	825.9	0.262	2.47392	0.06287	0.16284	0.00157	0.89	0.04708	0.0004	1802	51	973	9	1264	18	930	8	85
G01-14	145.68	1043.69	0.140	2.26945	0.05217	0.15134	0.00137	0.89	0.04382	0.00037	1779	46	908	8	1203	16	867	7	96
G01-15	112.61	836.62	0.135	4.00312	0.09078	0.25649	0.00239	0.9	0.07485	0.00189	1850	27	1472	12	1635	18	1459	36	26
G01-16	6344.22	9936.27	0.638	1.35343	0.0658	0.10733	0.00108	0.86	0.03164	0.00036	1456	97	657	6	869	28	630	7	122
G01-17	315.13	4804.09	0.066	0.31243	0.0729	0.03946	0.0006	0.89	0.01225	0.00771	508	461	250	4	276	56	246	154	103
G01-18	227.12	2256.38	0.101	0.7967	0.0212	0.05572	0.00052	0.88	0.01621	0.00029	1691	53	350	3	595	12	325	6	383
G01-19	179.56	1472.11	0.122	1.42625	0.03695	0.09963	0.00092	0.88	0.02898	0.00041	1694	52	612	5	900	15	577	8	177
G01-20	158.31	1345.57	0.118	1.80784	0.04898	0.12414	0.00119	0.88	0.03605	0.00057	1725	54	754	7	1048	18	716	11	129
TG17-04																			
T04-1	158	3247	0.049	0.4511	0.0131	0.03322	0.00033	0.88	0.00972	0.00028	1596	59	211	2	378	9	195	6	656
T04-2	157	2668	0.059	0.59538	0.01753	0.04432	0.00045	0.88	0.01298	0.00029	1575	60	280	3	474	11	261	6	463
T04-3	162	3014	0.054	0.32771	0.01088	0.02443	0.00026	0.87	0.00715	0.00024	1573	67	156	2	288	8	144	5	908
T04-4	165	495	0.332	4.59469	0.13566	0.29816	0.00312	0.89	0.08608	0.00078	1828	58	1682	16	1748	25	1669	14	9
T04-5	172	698	0.246	4.68336	0.13452	0.30945	0.00319	0.89	0.0895	0.00081	1796	57	1738	16	1764	24	1733	15	3
T04-6	132	756	0.174	4.84516	0.13377	0.31446	0.0032	0.89	0.09079	0.00081	1828	55	1763	16	1793	23	1756	15	4
T04-7	12,581	2208	5.556	1.48595	0.04156	0.08169	0.00085	0.9	0.00269	0.00007	2123	34	506	5	925	17	54	1	320

Table 1. Cont.

Sample	Concentrations (ppm)			Isotopic Ratios						Isotopic Age (Ma)						D (%)				
	Spot	Th, ppm	U, ppm	Th/U	<sup>207</sup> Pb/ <sup>235</sup> U	1s	<sup>206</sup> Pb/ <sup>238</sup> U	1s	Rho	<sup>208</sup> Pb/ <sup>232</sup> Th	1s	<sup>207</sup> Pb/ <sup>206</sup> Pb	1s	<sup>206</sup> Pb/ <sup>238</sup> U	1s		<sup>207</sup> Pb/ <sup>235</sup> U	1s	<sup>208</sup> Pb/ <sup>232</sup> Th	1s
T04-8		76	838	0.09	3.56987	0.10682	0.23785	0.00247	0.88	0.06885	0.00096	1780	59	1376	13	1543	24	1346	18	29
T04-9		160	1278	0.125	1.60385	0.08011	0.12603	0.00141	0.86	0.03711	0.00163	1474	100	765	8	972	31	737	32	93
T04-10		168	1056	0.159	2.55691	0.09559	0.18076	0.00195	0.87	0.05265	0.00101	1672	74	1071	11	1288	27	1037	19	56
T04-11		106	900	0.118	3.37205	0.11144	0.21691	0.00233	0.88	0.06257	0.00105	1844	64	1266	12	1498	26	1227	20	46
T04-12		384	685	0.562	4.26481	0.13656	0.26401	0.00301	0.9	0.0774	0.0022	1913	41	1510	15	1687	26	1507	41	27
T04-13		99	731	0.135	3.87204	0.13845	0.25613	0.00295	0.88	0.07409	0.00102	1794	70	1470	15	1608	29	1445	19	22
T04-14		135	1821	0.074	0.65278	0.07902	0.06792	0.00095	0.87	0.02062	0.00362	920	263	424	6	510	49	413	72	117
T04-15		130	312	0.418	5.13002	0.17986	0.32717	0.00409	0.9	0.1073	0.0034	1860	45	1825	20	1841	30	2060	62	2
T04-16		454	2027	0.224	1.37574	0.06037	0.09683	0.00115	0.88	0.02819	0.00043	1680	86	596	7	879	26	562	8	182
T04-17		187	660	0.282	4.99551	0.17298	0.31413	0.00379	0.9	0.06667	0.00219	1885	45	1761	19	1819	29	1305	41	7
T04-18		194	995	0.195	2.67808	0.11451	0.18011	0.00217	0.88	0.05219	0.00082	1763	83	1068	12	1322	32	1028	16	65
T04-19		1035	2874	0.36	0.29565	0.02673	0.02664	0.00037	0.87	0.00796	0.00019	1209	187	169	2	263	21	160	4	615
T04-20		1330	2466	0.541	1.11795	0.06348	0.06608	0.00089	0.89	0.0189	0.00026	1996	107	413	5	762	30	378	5	383
T04-21		204	950	0.215	2.5851	0.10676	0.16421	0.00206	0.88	0.04731	0.00057	1867	80	980	11	1296	30	934	11	91
T04-22		111	1132	0.098	2.47107	0.11625	0.17349	0.00221	0.88	0.05049	0.00149	1684	92	1031	12	1264	34	996	29	63
T04-23		149	1433	0.104	1.3872	0.08239	0.10273	0.00137	0.87	0.03006	0.00144	1585	117	630	8	884	35	599	28	152
T04-24		80	662	0.121	4.47254	0.17351	0.29298	0.00371	0.89	0.08467	0.00096	1811	76	1656	18	1726	32	1643	18	9
T04-25		255	1719	0.148	1.22536	0.05996	0.08258	0.00109	0.88	0.02393	0.0005	1759	95	512	6	812	27	478	10	244
T04-26		122	1217	0.1	2.22075	0.1074	0.15227	0.00202	0.88	0.04421	0.00119	1728	94	914	11	1188	34	874	23	89
T04-27		254	1177	0.216	2.22061	0.1068	0.14954	0.00202	0.88	0.04334	0.00061	1761	94	898	11	1188	34	857	12	96
T04-28		111	873	0.127	3.26508	0.13613	0.21155	0.00282	0.88	0.06107	0.00073	1831	81	1237	15	1473	32	1198	14	48
T04-29		319	923	0.346	3.63005	0.14934	0.22419	0.00303	0.9	0.06585	0.00253	1918	54	1304	16	1556	33	1289	48	47
T04-30		16,623	5388	3.125	0.60182	0.02499	0.0248	0.00034	0.9	0.00347	0.00013	2616	51	158	2	478	16	70	3	1556
T04-31		805	1878	0.429	1.0738	0.06265	0.07552	0.0011	0.88	0.02198	0.00027	1681	114	469	7	741	31	439	5	258
TG04-1		244	1565	0.156	1.75615	0.05519	0.1154	0.00119	0.88	0.03336	0.00045	1805	62	704	7	1029	20	663	9	156
TG04-2		77	678	0.113	4.6854	0.1299	0.30166	0.00313	0.89	0.08702	0.0008	1843	55	1700	16	1765	23	1687	15	8
TG04-3		118	795	0.148	4.34466	0.12103	0.28039	0.00288	0.89	0.0809	0.00073	1838	55	1593	14	1702	23	1572	14	15
TG04-4		267	840	0.317	3.99452	0.11283	0.25358	0.00266	0.9	0.07443	0.00193	1868	36	1457	14	1633	23	1451	36	28
TG04-5		266	778	0.341	4.18944	0.12207	0.26964	0.00292	0.9	0.05883	0.00163	1843	37	1539	15	1672	24	1155	31	20
TG04-6		149	118	1.266	11.71573	0.36769	0.43507	0.00556	0.9	0.07324	0.00208	2787	35	2329	25	2582	29	1429	39	20
TG04-7		143	954	0.15	2.59705	0.0917	0.18474	0.002	0.88	0.05384	0.00087	1660	70	1093	11	1300	26	1060	17	52
TG04-8		255	1450	0.176	12.34339	0.34999	0.28834	0.00303	0.9	1.20221	0.03048	3523	31	1633	15	2631	27	15,957	280	116
TG04-9		2296	1278	0.746	0.83411	0.02466	0.04627	0.0005	0.9	0.01101	0.00029	2108	37	292	3	616	14	221	6	622
TG04-10		468	2388	0.196	0.83616	0.03891	0.06175	0.00071	0.87	0.01806	0.00043	1591	92	386	4	617	22	362	9	312
TG04-11		512	1715	0.299	1.54885	0.13922	0.11537	0.0016	0.88	0.03378	0.00153	1574	176	704	9	950	55	672	30	124
TG04-12		840	1590	0.529	2.11849	0.06375	0.11755	0.00128	0.9	0.03194	0.00086	2107	37	716	7	1155	21	635	17	194

D—degree of discordance,  $D = 100 \{ [t(^{207}\text{Pb}/^{206}\text{Pb})] / [t(^{206}\text{Pb}/^{238}\text{U})] - 1 \}$ . Rho—correlation coefficient of ratios  $^{207}\text{Pb}/^{235}\text{U} - ^{206}\text{Pb}/^{238}\text{U}$ .

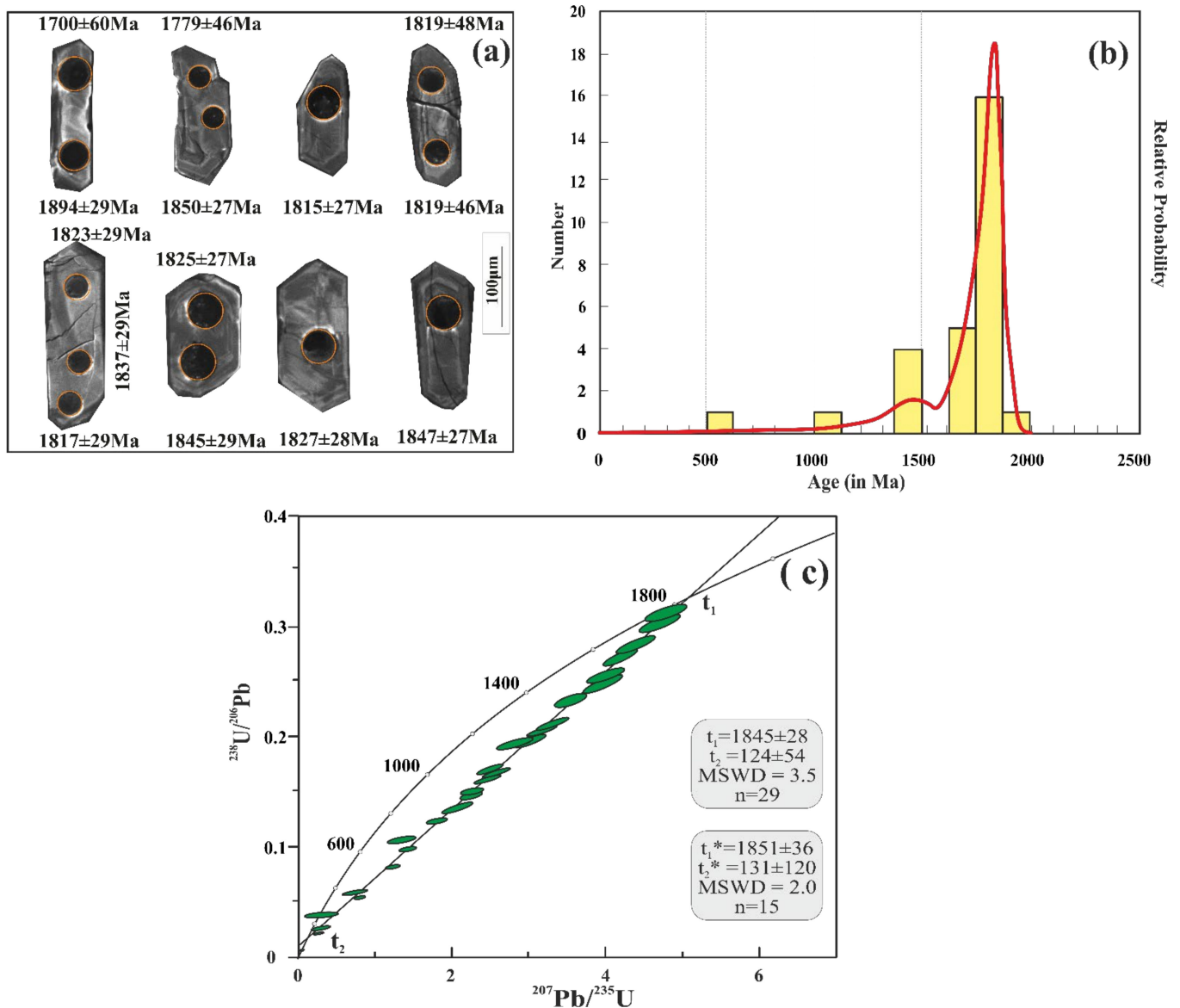


**Figure 6.** Zircon of granite TG17-01. (a) Cathodoluminescence (CL) images of representative zircon grains. Numbers of analytical points:  $^{207}\text{Pb}/^{206}\text{Pb}$  ages (in Ma). (b) Histogram of  $^{207}\text{Pb}/^{206}\text{Pb}$  age distribution in Sample TG17-01. (c) U–Pb diagram with a concordia for zircons from the granite (Sample TG17-01). The U–Pb age ( $t$ ) of magmatic zircons is  $1851 \pm 36$  Ma ( $t_1^*$ ) for zircon with  $D < 100\%$  and  $1845 \pm 28$  Ma ( $t_1$ ) for all analytical points. ( $t_1$ —the upper intersection of discordia age;  $t_2$ —the lower intersection of discordia age).

Sample TG17-04 contains two morphological types of zircon grains: (1) sub-idiomorphic grains are present, and idiomorphic prismatic crystals of zircon type or their parts, often with oscillation zoning, retaining or partially retaining dipyrmaid facets, are less common; (2) ellipsoidal grains with rounded facets. Morphological (zircon) type 1 occurs as transparent to semi-transparent light-colored crystals with a short prismatic habit. Zircons of this type make up approximately 80–90% of the total volume of this mineral in the rock. The grains vary from 60 to 200  $\mu\text{m}$ , and their elongation coefficient is 1–2. The crystal form is due to the development of prisms and dipyrramids. A microprobe study of zircons in BSE and CL shows that grains are relatively well-preserved. The surface of the zircon grains displays various degrees of longitudinal–transverse fracturing; grains with a smooth surface and with no fractures are less common. The internal structure of some of the grains is multizonal; the

zones are distributed symmetrically (Figure 7a). There are three metamictic grains with dark CL or with dark micro-veins only.

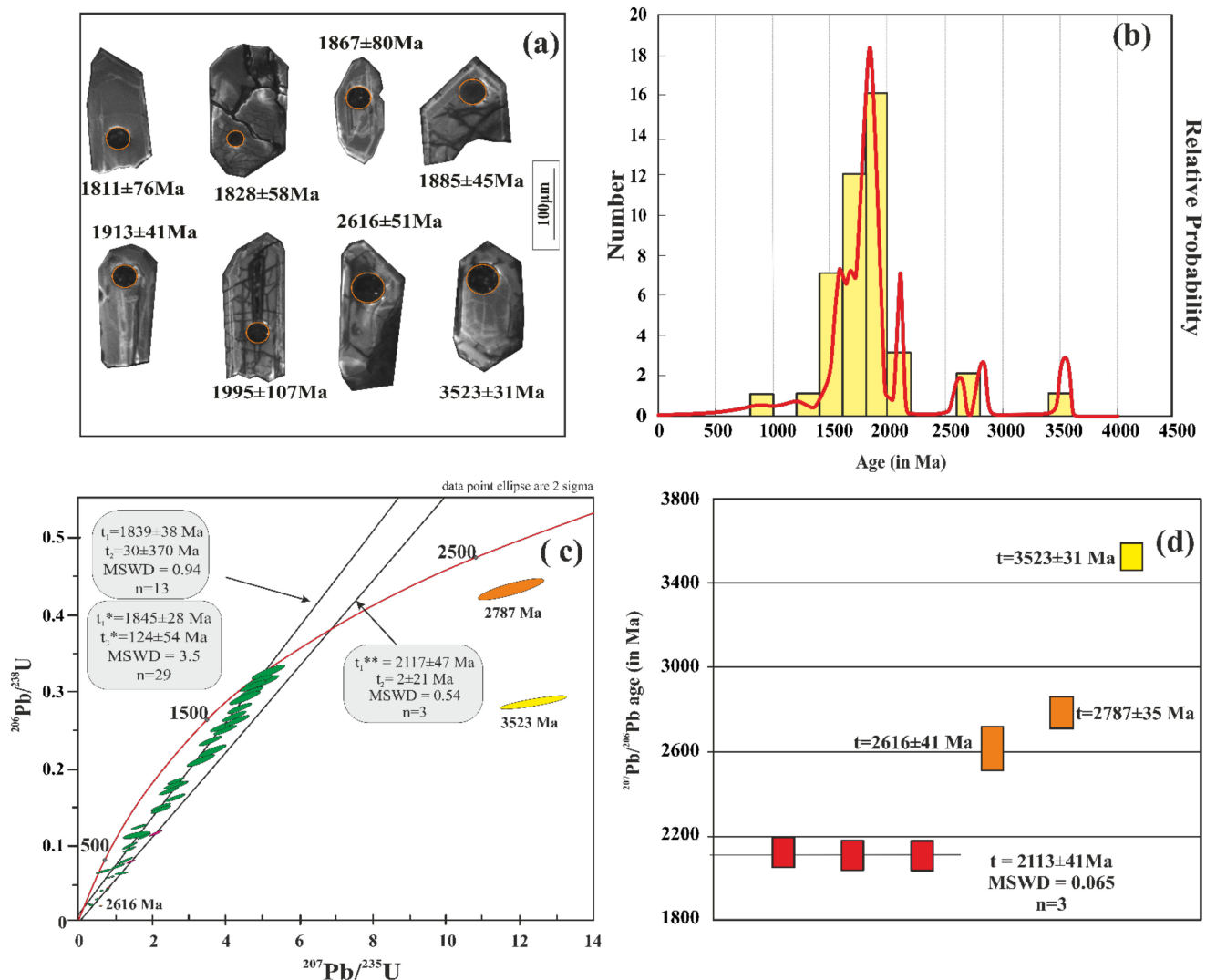


**Figure 7.** Zircon of granite TG17-04. (a) Cathodoluminescence (CL) images of representative zircon grains. Numbers of analytical points:  $^{207}\text{Pb}/^{206}\text{Pb}$  ages (in Ma). (b) Histogram of  $^{207}\text{Pb}/^{206}\text{Pb}$  age distribution in Sample TG17-04. (c) U–Pb diagram with a concordia for Paleoproterozoic (yellow), Neoproterozoic (orange), Paleoproterozoic core (red), and Paleoproterozoic magmatic (green) zircons from the granite (Sample TG17-04);  $t_1$ —the upper intersection of discordia age;  $t_2$ —the lower intersection of discordia age;  $t_1$ —1839 ± 38 Ma is the age for magmatic zircon with  $D < 30\%$ ,  $t_1^*$ —1845 ± 28 Ma is age all analytical points of magmatic zircons,  $t_1^{**}$ —2117 ± 47 Ma is the age of Paleoproterozoic core; with  $D < 30\%$  (red color) is 1839 ± 38 Ma ( $t_1$ ), and for all (pink are zircon with  $D > 30\%$ ) analytical points are 1845 ± 28 Ma ( $t_1^*$ ). ( $t_1$ —the upper intersection of discordia age;  $t_2$ —the lower intersection of discordia age); (d) Weighted average  $^{207}\text{Pb}/^{206}\text{Pb}$  age of zircons with age older 1.95 Ga (color are same as in 7c).

A second morphological type of zircon occurs as ellipsoidal grains with subdued outlines, with no dipyrmaid facets characteristic of type 1. Such grains are less common, amounting to 10–20% in the rock and forming light-yellow semi-transparent crystals, no more than 80 μm in size. The grain surface is dull, rough, and displays minor transverse fracturing. The internal structure in BSE is homogeneous.

The internal structure of these two morphotypes displays the presence (in some cases) of complex crystals with homogeneous internal cores that are well-defined in CL images (Figure 7a). In zircons of type 2, cores occupy two thirds of the entire grain volume, and their shape is markedly different from the external rim. This is also indicated by the higher

idiomorphism and the presence of clearly traceable prismatic facets. There are mineral inclusions in the internal zone (core). However, these are too small (less than 3  $\mu\text{m}$ ) to be reliably identified. The cores of zircons of morphotype 1 are less conspicuous, and their shape is consistent with the external rim; the core structure in a CL image is more homogeneous. The zircons of both morphological types typically display solid-phase biotite, thorite, monazite, and apatite inclusions in both the central and marginal portions of grains. In addition, zircon–quartz intergrowths are encountered.

### 5.2. U–Th–Pb Isotope Data from Zircons

U–Th–Pb age isotope LA–ICP–MS analysis was performed on 29 points from 17 grains in Sample TG17-01 and 43 points from 37 zircon grains in Sample TG17-04 (Table 1). The  $^{207}\text{Pb}/^{206}\text{Pb}$  age of most TG17-01 zircons is 2.0–1.6 Ga, with a maximum of approximately 1.8 Ga (Figure 6b; Table 1). All analytical points are formed on the U–Pb diagram with a concordia single isochron line—discordia (Figure 6c)—as is common for discordant U–Pb age data [38]. The line plotted using all analytical points ( $n = 29$ ) has an upper intersection with concordia at  $1846 \pm 26$  Ma and a lower intersection at  $108 \pm 40$  Ma (Figure 6c). If only analytical points with a discordance ( $D$ , Table 1) of less than 100% ( $D < 100\%$ ) are used to estimate U–Pb age by the upper intersection at  $1851 \pm 36$  Ma, the lower value at  $131 \pm 120$  Ma (MSWD = 2.0,  $n = 15$ ) (Figure 6c) is obtained. This  $1851 \pm 36$  Ma age can be regarded as the most precise crystallization age of zircons in TG17-01 granite, and  $108 \pm 40$  Ma is the age of Pb lost during tectonic events.

The  $^{207}\text{Pb}/^{206}\text{Pb}$  age of most TG17-04 zircons is 2.0–1.6 Ga, with a maximum of approximately 1.8 Ga (Figure 7b; Table 1). However, there are three peaks with ages of (1) 3.5 Ga, (2) 2.62 and 2.78 Ga, and (3) ca. 2.1 Ga (Figure 7c; Table 1). All analytical points (excluding those older than 1.95 Ga) are formed on the U–Pb diagram with a concordia single isochron line (Figure 7c), as is common for discordant U–Pb age data [44]. The U–Pb age of the most common group of zircons (Figure 7c), estimated from the upper intersection with discordia using all analytical points, is  $1845 \pm 28$  Ma, and the lower intersection of  $124 \pm 54$  Ma. This first age is consistent with the magmatic stage of granite formation and the second with an age of terminal tectonic events. Using the most concordant values ( $D < 30\%$ ), the upper intersection of discordia is estimated as  $1839 \pm 38$  Ma (Figure 7c). There is also the existence of analytical points of the core with older ages: the Paleoproterozoic (2.1 Ga), Neoproterozoic (2.62 Ga and 2.78 Ga), and Paleoproterozoic (3.52 Ga). These data indicate that the protolith of these granites contained detrital zircons of different ages, possibly as redeposited clasts.

### 5.3. Zircon Geochemistry

The geochemical characteristics of the zircons discussed are also consistent with their magmatic genesis. The analytical points of zircon composition on the discrimination diagrams Y–U, Ce/Ce\*, and Eu/Eu\* [5] are in the granite (leucogranite) fields (Figure 8). This means that the composition of zircons did not change significantly, despite the loss of Pb.

The average  $\Sigma\text{La–Lu}$  and Y concentrations in zircons from both granite samples analyzed (3200 and 5500 ppm, respectively) are slightly higher than those in zircons from granites [1]. However, there is a significant difference in the composition of zircons with different degrees of discordance ( $D$ ): zircons with  $D > 100$  are enriched with REE and Y. Some differences in the composition of zircons from the two samples discussed are also noteworthy.

The Th and U contents of TG17-01 zircons ( $D < 100\%$ ) are relatively high (average 202 ppm (Th) and 805 ppm (U)), but if using grains with  $D > 100\%$  (Table 1) too, the average values are 514 ppm (Th) and 2150 ppm (U). The average Th/U ratio is 0.22 (Table 2), which is characteristic of magmatic zircon [1]. Chondrite-normalized REE concentrations in zircons from Sample TG17-01 are similar to those in granites (Figure 9a): the REE distribution spectrum is differentiated, with an increase from La to Lu, HREE enrichment ( $(\text{Yb}/\text{Sm})_{\text{N-16}}$ (avg.)), and positive cerium ( $\text{Ce}/\text{Ce}^*-2$ (avg.)) and negative europium ( $\text{Eu}/\text{Eu}^*-0.05$ (avg.))

anomalies. REEs are enriched in zircons with  $D > 100\%$  (Figure 9a). The average crystallization temperature of these zircons, determined using a Ti thermometer [44], is estimated to be  $864\text{ }^{\circ}\text{C}$  (this average does not include zircons with  $D > 100\%$ ), which could be a hot minimum melt temperature for granite [45].

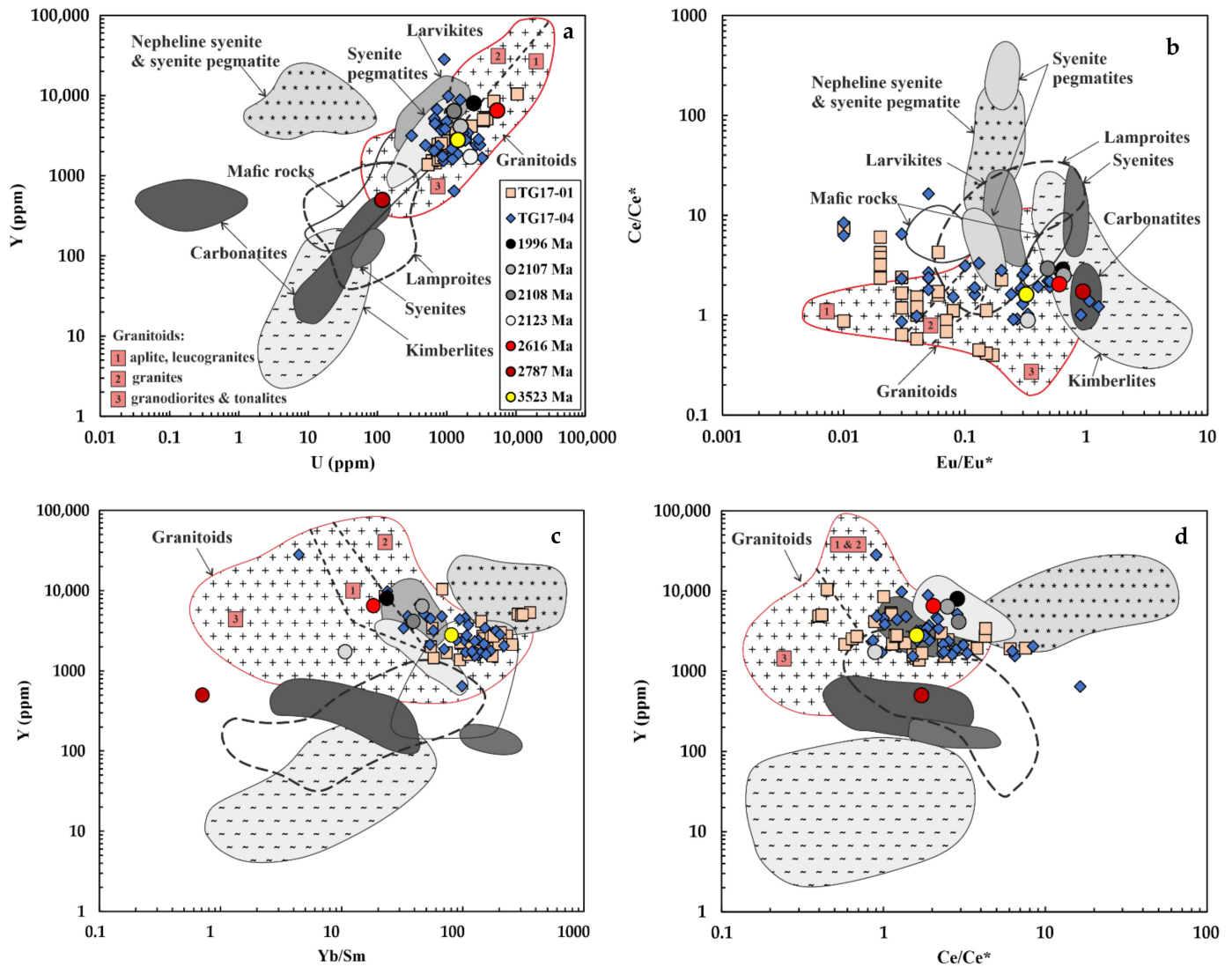


**Figure 8.** Analytical points of zircons from Lesser Garhwal Himalaya 1.85 Ga granite (TG17-01 and TG17-04). (a) U versus Y; (b) Europium anomaly ( $\text{Eu}/\text{Eu}^*$ ) versus Cerium anomaly ( $\text{Ce}/\text{Ce}^*$ ); (c) Yb/Sm versus Y; and. (d) Cerium anomaly ( $\text{Ce}/\text{Ce}^*$ ) versus Y. (Trace element composition in ppm). Pink squares—all zircons from TG17-01 granite (1: aplite, leucogranites; 2: granites; 3: granodiorites and tonalites); blue rhombus—zircons from TG17-04 granite with an age of ca. 1850 Ma; circles—zircons, with age greater than ca. 1850 Ma from TG17-04 granite. The fields of zircon composition from different rock types are taken from [5].

**Table 2.** Trace element concentrations (in ppm) of Th/U, Eu/Eu\*, Ce/Ce\*, and T °C for zircons from Lesser Garhwal Himalaya (India) granite TG17-01 and TG17-04.

Sample	Y	La	Ce	Pr	Nd	Sm	Eu	Gd	Tb	Dy	Ho	Er	Tm	Yb	Lu	ΣLa-Lu	Eu/Eu*	Ce/Ce*	Ti	T °C**	Th/U
TG17-01																					
T01-1	1943.03	0.049	2.54	0.114	1.56	4.52	0.05	26.36	12.03	164.16	64.17	289.46	61.42	571.13	94.62	1292.18	0.01	7.52	8.01	722	0.241
T01-2	1454.44	1.228	6.51	0.68	5.59	6.89	0.282	29.63	11.22	132.5	48.9	212.47	43.31	394.93	69.98	964.12	0.06	1.58	32.34	856	0.562
T01-3	2185	0.452	1.84	0.288	2.3	4.53	0.151	27.56	13.11	174.81	70.68	320.09	68.04	635.55	110.88	1430.28	0.04	1.14	39.02	877	0.151
T01-4	1907.11	0.0314	1.447	0.085	1.43	3.26	0.056	22.85	10.99	151.99	61.19	280.95	60.46	563.91	99.33	1257.98	0.02	6.06	12.4	760	0.144
T01-5	2746.23	0.073	1.55	0.091	1.08	3.91	0.057	29.6	15.13	216.77	89.59	428.24	94.57	905.84	160.9	1947.4	0.02	4.24	15.16	779	0.129
T01-6	5346.78	0.68	2.73	0.439	3.56	5.63	0.381	38.32	24.1	380.13	163.2	824.2	200.61	2022.89	362.71	4029.58	0.08	1.11	87.53	976	0.043
T01-7	5124.78	1.14	4.98	0.864	5.77	7.1	0.76	35.91	22.47	353.24	153.06	787.94	194.74	2013.76	374.18	3955.91	0.15	1.12	157.51	1059	0.043
T01-8	4885.93	6.55	7.1	2.41	12.44	7.62	0.849	29.98	17.07	280.35	135.02	777.33	203.54	2301.55	466.83	4248.64	0.17	0.40	184.64	1084	0.091
T01-9	5039.9	6.17	7.03	2.29	11.97	7.63	0.736	29.94	17.41	289.95	139	791.96	210.68	2386.66	480.31	4381.74	0.15	0.42	220.29	1112	0.078
G01-1	2470.52	0.308	3.91	0.394	3.94	7.06	0.082	39.46	16.54	210.21	81.22	357.92	74.19	677.34	116.5	1589.7	0.02	2.50	87.03	975	0.330
G01-2	10,455.74	54.32	72.75	24.03	119.7	61.93	3.82	132.11	51.93	685.91	302.99	1653.66	415.49	4194.05	791.48	8564.17	0.13	0.45	1055.76	1428	0.245
G01-3	1538.22	0.177	1.405	0.095	1.154	2.72	0.066	17.88	8.68	120.51	48.94	231.11	50.22	477	84.02	1043.98	0.03	2.39	61.08	929	0.172
G01-4	3412.43	0.296	8.21	0.615	7.74	13.86	0.672	77.24	28.3	333.65	116.71	475.52	90.05	776.89	129.24	2058.99	0.06	4.27	26.59	835	0.390
G01-5	1938.66	0.254	4.12	0.231	2.8	4.77	0.094	28.76	12.67	166.81	63.64	281.45	58.51	534.45	89.19	1247.75	0.02	3.78	24.15	825	0.255
G01-6	2258.43	2.45	10.34	1.161	6.77	7.01	0.194	33.2	14.2	183.19	73.44	342.03	71.54	666.04	123.46	1535.2	0.04	1.36	7.54	717	0.287
G01-7	2166.23	0.785	1.298	0.318	2.31	3.34	0.103	22.11	11.22	158.99	66.36	322.72	69.66	656.25	121.91	1437.37	0.04	0.58	13.01	764	0.108
G01-8	2126.92	0.1	1.221	0.134	1.08	2.65	0.044	20.4	10.38	147.55	64.14	315.08	70.15	678.1	125.52	1436.55	0.02	2.35	17.19	791	0.086
G01-9	1379.93	0.664	3.73	0.375	3.11	4.34	0.107	21.59	9.15	115.07	45.45	209.66	44.39	409.97	77.52	945.13	0.03	1.66	98.77	992	0.382
G01-10	2005.28	0.468	7.3	0.546	6.32	9.3	0.1	42.43	15.3	179.69	65.48	281.32	56.44	506.98	93.38	1265.5	0.02	3.21	115.52	1014	0.812
G01-11	1597.94	1.129	5.48	0.57	4.05	4.27	0.113	21.8	9.78	128.15	50.77	232.63	50.38	472.3	82.31	1063.73	0.04	1.52	7.61	717	0.198
G01-12	3008.48	0.218	2.58	0.293	2.14	4.61	0.728	27.72	15.07	216.56	89.97	437.33	97.72	949.75	165.35	2010.4	0.2	2.27	9.29	734	0.096
G01-13	1688.41	1.055	7.57	0.898	6.15	6.84	0.271	29.15	11.44	137.03	51.65	234.37	50.67	503.39	96.48	1136.96	0.06	1.73	75.73	957	0.262
G01-14	2722.56	0.259	1.358	0.253	2.41	4.7	0.131	34.83	17.05	222.5	83.99	370.3	75.59	682.8	115.13	1611.3	0.03	1.18	44.48	891	0.140
G01-15	2537.3	0.491	0.999	0.242	1.99	4.57	0.125	31.12	15.22	204.24	78.96	356.03	74.12	681.99	117.82	1567.92	0.03	0.64	44.36	891	0.135
G01-16	133,145	145.68	640.52	183.33	1730.53	2135.34	7.39	6344.85	2010.36	17,523.39	4379.9	12,927.88	1757.83	11,167.7	1380.76	62,335.46	0.01	0.87	20.94	810	0.638
G01-17	8533.28	15.99	69.98	15.07	102.92	79.99	1.732	224.1	82.09	870.02	270.83	1065.95	207.2	1815.67	299.76	5121.3	0.04	1.00	9.87	740	0.066
G01-18	4164.55	7.9	20.43	3.35	17.12	9.43	0.413	37.23	18.91	285.95	123.37	614.19	138.18	1341.2	254.89	2872.56	0.07	0.88	1314.76	1484	0.101
G01-19	2813.09	1.2	5.3	0.793	5.18	5.54	0.176	27.72	14.04	203.74	86.73	427.06	95.84	941.36	173.91	1988.59	0.04	1.21	1633.04	1543	0.122
G01-20	2720.76	6.17	12.59	2.71	13.74	7.08	0.333	28.05	12.6	177.6	78.85	443.9	114.2	1265.43	266.94	2430.19	0.07	0.68	2387.36	1657	0.118
TG17-04																					
T04-1	4787.24	8.64	40.14	4.85	26.62	18.18	11.86	64.71	29.99	392.93	148.35	648.69	135.34	1224.29	194.85	2949.44	1.06	1.38	14.37	774	0.049
T04-2	4577.67	9.12	26.41	3.75	17.54	11.11	6.71	46.84	25.29	357.41	141.42	627.27	132.57	1163.96	182.14	2751.54	0.9	1.00	8.38	726	0.059
T04-3	4384.91	9.68	36.38	4.58	21.33	11.98	9.7	46.99	24.4	346.85	134.39	603.96	126.56	1132.59	179.18	2688.57	1.26	1.21	8.78	730	0.054
T04-4	1549.1	0.14	3.67	0.114	1.6	3.32	0.096	22.43	9.88	126.27	51.24	230.12	48.54	447.58	78.42	1023.42	0.03	6.48	14.47	774	0.333
T04-5	1678.88	0.239	3.37	0.217	1.65	3.64	0.38	23.51	10.68	138.16	54.2	246.23	51.92	475.45	83.57	1093.22	0.13	3.30	8.08	722	0.246
T04-6	1779.73	0.032	1.281	0.0629	0.97	3.1	<0.036	21.64	10.56	145.77	57.62	268.18	57.07	526.62	94.34	1187.26	0.01	6.25	5.48	691	0.175
T04-7	1728.96	8.52	29.79	6.53	39.58	32.64	5.42	79.38	24.11	203.08	56.76	211.45	39.84	349.27	59.24	1145.61	0.33	0.89	124.54	1025	5.698

Table 2. Cont.

Sample	Y	La	Ce	Pr	Nd	Sm	Eu	Gd	Tb	Dy	Ho	Er	Tm	Yb	Lu	ΣLa-Lu	Eu/Eu*	Ce/Ce*	Ti	T °C**	Th/U
T04-8	1672.77	0.183	1.51	0.117	1.12	3.31	0.097	22.8	10.94	139.18	53.13	232.04	50.1	462.5	79.83	1056.86	0.03	2.31	5.05	684	0.091
T04-9	2422.57	1.7	10.48	1.226	6.64	6.27	1.042	29.12	13.85	191.34	76.73	341.48	71.45	646.21	106.25	1503.79	0.24	1.61	7.07	711	0.125
T04-10	2423.42	1.81	13.63	1.38	8.7	7.68	2.06	32.37	14.92	196.34	77.34	349.76	73.45	680.73	112.65	1572.82	0.4	1.92	8.68	729	0.159
T04-11	2408.28	0.795	2.02	0.343	2.34	4.45	0.12	30.58	14.8	193.38	74.32	324.14	67.24	599.75	101.47	1415.75	0.03	0.86	24.48	826	0.118
T04-12	2121.58	0.558	7.92	0.574	5.32	8.83	0.635	41.67	16.51	193.51	68.29	276.18	54.57	472.74	74.61	1221.92	0.1	3.11	24.51	826	0.561
T04-13	2346.14	0.573	6.57	0.582	3.91	4.94	1.17	30.08	14.59	188.96	73.99	329.13	67.89	622.1	105.66	1450.14	0.3	2.53	20.39	808	0.135
T04-14	3724.12	2.88	22.32	2.34	12.69	9.95	3.26	39.85	20.23	281.93	113.6	531.87	116.61	1103.77	189.23	2450.53	0.5	1.91	23.94	824	0.074
T04-15	645.11	0.045	5.03	0.101	0.97	1.86	0.072	11.65	4.53	56.09	21.96	97.88	19.88	183.34	32.8	436.21	0.05	16.40	11.27	751	0.417
T04-16	9788.89	31.3	120.72	13.72	78.5	77.7	14.6	283.42	100.7	996.38	304.07	1161.42	219.1	1853.5	309.99	5565.12	0.3	1.29	93.65	985	0.224
T04-17	1536.48	0.846	3.96	0.399	2.21	3.53	0.205	19.68	9.03	118.53	48.72	226.48	47.12	443.02	82.39	1006.12	0.08	1.52	8.86	730	0.283
T04-18	4801.98	51	89.1	9.32	38.39	21.25	4.92	151.44	61.91	554.8	146.11	495.5	87.23	747.31	128.06	2586.34	0.27	0.91	15.94	784	0.195
T04-19	6715.6	6.94	82.14	7.27	42.44	35.53	12.98	118.67	48.5	568.63	210.45	903.52	176.59	1555	270.2	4038.86	0.61	2.57	98.53	992	0.360
T04-20	8001.98	8.56	123.45	10.73	67.11	62	22.98	196.61	70.32	743.07	242.1	944.4	174.91	1463.46	237.74	4367.44	0.64	2.86	86.66	974	0.539
T04-21	3181.39	2.26	16.19	1.99	12.1	12.93	2.53	55.21	23.33	272.89	98.2	416.95	81.73	740.78	131.26	1868.35	0.29	1.70	45.51	894	0.215
T04-22	3156.92	0.706	4.4	0.525	3.28	4.79	0.476	29.87	16.2	228.24	96.44	455.47	96.53	900.66	164.39	2001.98	0.12	1.61	22.09	816	0.098
T04-23	3425.49	1.85	13.29	1.37	7.63	6.67	1.44	33.86	18.19	256.03	106.69	505.65	107.59	1017.16	185.93	2263.35	0.29	1.85	30.99	851	0.104
T04-24	2047.75	<0.0181	0.748	0.0396	0.81	2.7	<0.034	21.54	11.01	153.14	64.04	300.45	63.1	591.81	108.96	1318.37	0.01	8.39	4.94	682	0.121
T04-25	4720.47	4.72	45.9	4.87	28.32	21.62	7.62	65.18	28.85	363.05	136.16	597.17	120.1	1094.2	192.84	2710.6	0.62	2.13	80.79	965	0.148
T06-26	2846.5	0.445	3.15	0.338	2.28	3.9	0.181	27.53	14.49	208.45	86.68	404.5	85.71	793.74	143.89	1775.28	0.05	1.80	15.22	779	0.100
T06-27	3839.21	5.74	23.97	4.76	28.07	24.63	4.67	75.21	29.4	336.16	119.55	510.91	104.75	947.73	162.08	2377.63	0.33	1.02	14.66	776	0.216
T06-28	1717.84	0.715	1.86	0.251	2.04	3.68	0.13	25.13	11.98	145.67	53.72	221.74	44.2	388.7	64.78	964.6	0.04	0.98	12.8	763	0.127
T06-29	1862.31	1.08	14.37	1.21	7.28	7.34	0.97	29.54	12.64	156.07	59.92	264.91	55.95	515.2	89.84	1216.32	0.2	2.80	15.21	779	0.346
T04-30	6515.36	15.59	149.07	16.99	99.31	80.07	24.52	198.39	68.8	656.29	202.06	803.87	161.95	1464.89	244.91	4186.71	0.6	2.04	155.86	1058	3.085
T04-31	5166.56	3.66	48.39	3.87	24.54	24.92	5.4	107.09	40.67	461.55	166.39	688.66	135.81	1190.67	196.65	3098.27	0.32	2.86	53.42	913	0.429
TG04-1	3400.18	4.78	44.85	4.34	25.36	21.56	6.42	79.02	31.13	330.86	105.62	411.68	78.96	700.01	121.66	1966.25	0.48	2.19	34.11	862	0.156
TG04-2	1609.02	0.111	1.259	0.1	1.08	2.65	0.107	19.58	9.58	131.63	50.97	227.21	45.35	412.44	75.55	977.62	0.05	2.65	19.01	801	0.114
TG04-3	2160.45	0.291	3.02	0.285	1.85	3.99	0.169	25.57	12.31	167.7	67.07	311.25	64.59	598.28	109.91	1366.28	0.05	2.33	33.58	860	0.148
TG04-4	1746.49	0.653	6.07	0.498	3.37	3.93	0.174	27.8	11.22	143.06	55.54	250.21	51.02	469.37	85.43	1108.35	0.05	2.36	18.35	797	0.318
TG04-5	28,208.39	1.223	10.2	5.17	89.98	376.36	77.74	2340.43	813.06	5527.78	969.98	2106.02	251.81	1671.14	237.19	14478.08	0.25	0.90	171.7	1072	0.342
TG04-6	499.88	13.88	154.46	28.72	230.85	156.15	44.02	131.5	16.62	86.22	18.08	58.25	11.42	110.91	23.2	1084.28	0.94	1.72	59.27	926	1.263
TG04-7	2775.42	0.95	6.74	0.743	5.09	7.06	0.617	37.44	16.54	223.54	88.32	403.42	83.56	760.4	136.66	1771.08	0.12	1.78	51.11	908	0.150
TG04-8	2794.04	5.01	27.3	2.86	14.37	9.74	1.87	34.12	15.57	212.27	85.41	397.16	83.35	786.44	143.27	1818.74	0.32	1.60	15.08	778	0.176
TG04-9	6389.84	7.69	82.63	7.11	41.48	37.49	13.63	109.23	43.18	494.47	182.91	832.58	177.39	1737.5	340.64	4107.93	0.65	2.48	133.94	1035	1.797
TG04-10	8827.06	11.73	93.24	10.3	63.51	69.44	22.52	277.35	100.4	951.6	279.32	1040.29	192.07	1671.72	287.54	5071.03	0.5	1.89	159.15	1061	0.196
TG04-11	4480.42	4.4	42.64	4.34	24.81	20.28	6.97	68.47	29.99	372.03	140.38	610.02	122.44	1099.77	189.77	2736.31	0.57	2.17	24.51	826	0.299
TG04-12	4130.61	3.3	48.92	4.21	25.51	25.06	7.16	84.61	32.74	361.91	124.92	528.07	106	980.19	172.46	2505.06	0.48	2.92	57.02	921	0.528

1-sigma error for estimation of element concentration is 4–8%; \*\*T °C = (5080)/(6.01 – log (Ti)) – 273.15 [38].

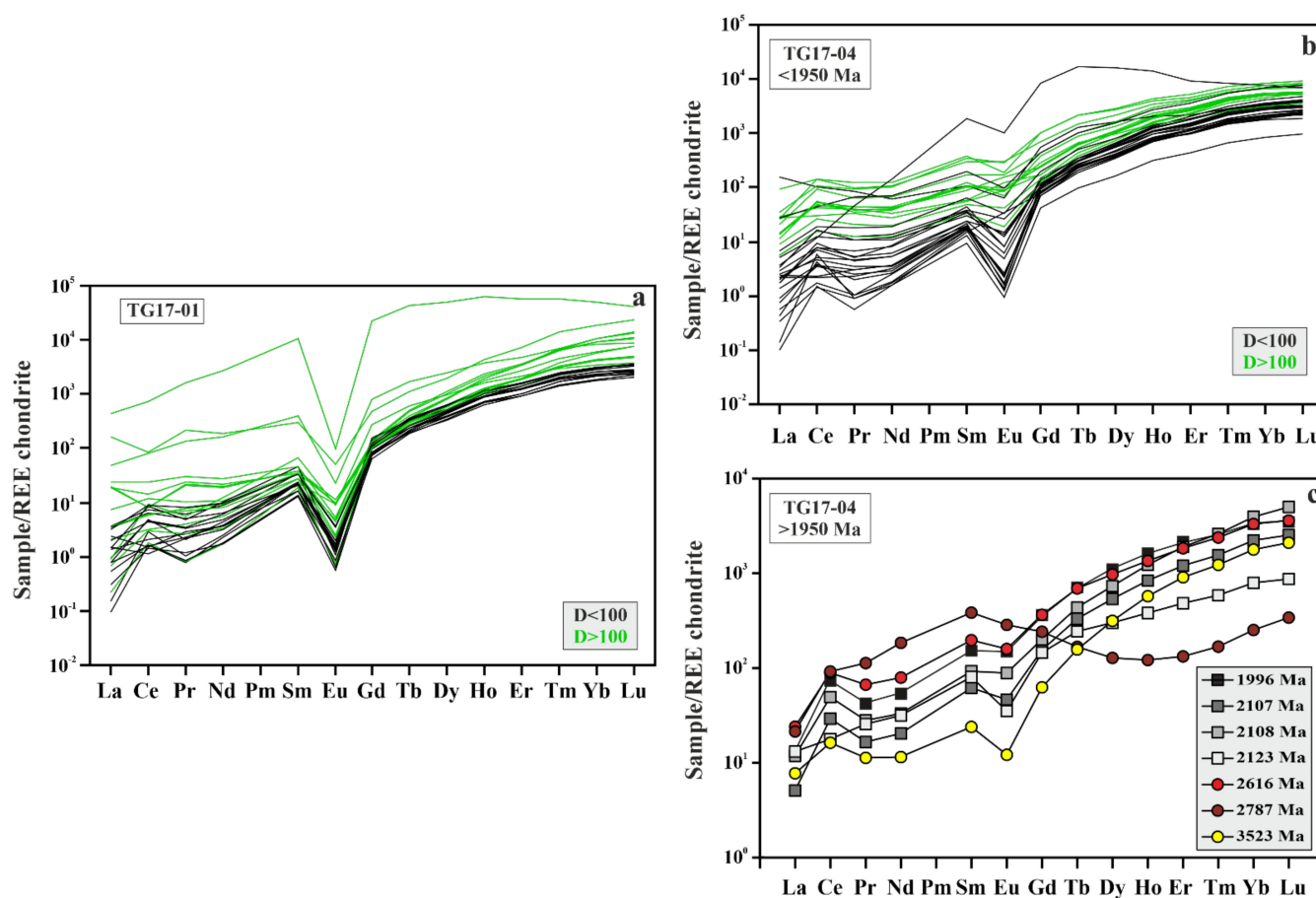


**Figure 9.** Chondrite-normalized [46] REE concentrations in zircons (a) from TG17-01 granite and (b,c) TG17-04 granite.

Chondrite-normalized REE concentrations in zircons from Sample TG17-04 are also similar to those in granites (Figure 9b) (Table S3): the REE distribution spectrum is differentiated, with an increase from La to Lu; HREE enrichment ( $(Yb/Sm)_N-151(\text{avg.})$ ) and positive cerium ( $Ce/Ce^*-2(\text{avg.})$ ) and negative europium ( $Eu/Eu^*-0.06(\text{avg.})$ ) anomalies are observed in TG17-01 zircons (Figure S5, Table S4). The average crystallization temperature of these zircons, determined using a Ti thermometer [45], is estimated to be 796 °C (this does not include zircons with  $D > 100\%$ ). Thus, 1.85 Ga zircons from Sample TG17-04 are a geochemically homogeneous group with parameters typical of granites, too, (Figure 8) (Figure S6).

The REE concentrations are typically igneous zircon with Lu concentrations 100 s of times greater than La, and all have a positive Ce anomaly and a negative Eu anomaly. Using D as a demarcation, the more discordant and TE-rich zircons have greater REE concentrations. For TG17-01, the high D zircons include the greatest Eu anomalies, suggesting that the zircons grew from a fractionating magma and that plagioclase was a significant fractionating phase. TG17-04 shows somewhat different behavior. In this sample, the most discordant have similar Eu anomalies.

Most of the zircon cores are plotted in the field of typical granitic magmas, and only the core with 2.78 Ga age shows a significant difference (spot TG04-6, Table 1), plotting in fields typical for carbonatites or mafic rocks (Figure 8). This core is notably depleted in HREE ( $(Yb/Sm)_N-0.66$ ), which likely indicates growth in the presence of garnet and possibly a metamorphic origin. Its crystallization temperature, determined using a Ti thermometer [46], is higher (926 °C) than that of the most common grains, which could be indirectly regarded as evidence of its metamorphic genesis. Thus, zircon cores from this sample are of both magmatic and metamorphic origin.

## 6. Discussion

The geochemical analysis of zircons from the studied granites has reliably identified them as magmatic. Most of the zircons have more than a 100% degree of discordance, which correlates with the enrichment of REE, U, and Th. However, in any case, all these zircons are discriminated as magmatic (Figure 8). The study of magmatic zircons from this granite can be used to precisely estimate the U–Pb age of the magmatic stage of granites formed:  $1839 \pm 38$  and  $1851 \pm 36$  Ma, respectively, for each of these samples. These values are identical within the constraints of the measurement accuracy. On the diagram with a concordia, all of the least discordant analytical points from both samples form a common isochron with an upper intersection of  $1845 \pm 19$  Ma (Figure 10). This age can be regarded as the most valid age for the magmatic stage formation of granites. The lower intersection at  $112 \pm 62$  Ma could be interpreted as the age of a thermal event during Indian plate subduction at ca. 80–60 Ma ago [9]. In the Paleoproterozoic era, many granites formed in the Himalayas from 1980 to 1750 Ma [12,47–49] (Figure 11), and the 1.85 Ga Chail Group granites in the Garhwal Lesser Himalaya continue to be essential for any geological reconstructions.

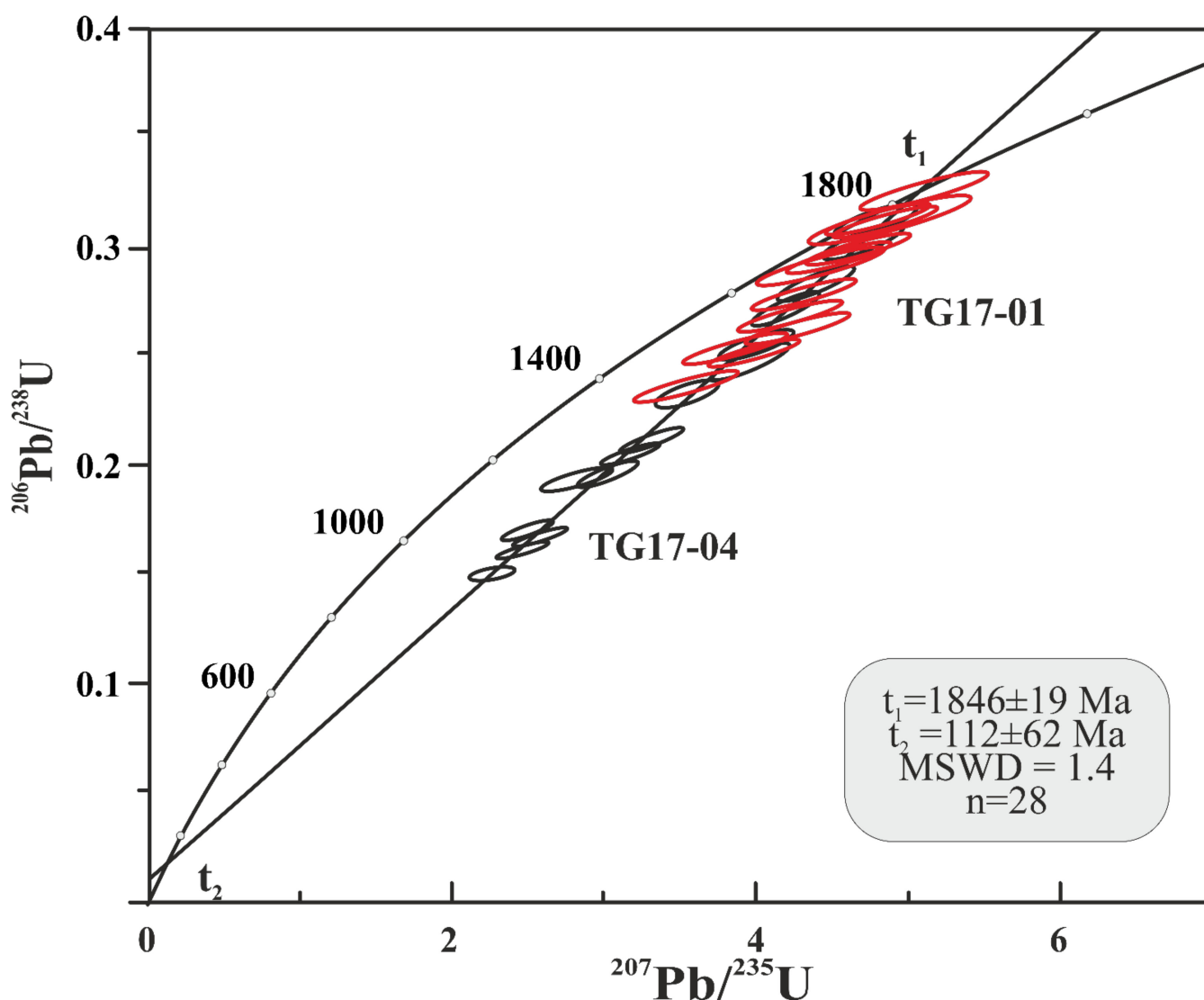


**Figure 10.** Diagram with a concordia for zircons from granite (Sample TG17-01—red and TG17-04—black). U–Pb age magmatic zircons are  $1845 \pm 19$  Ma.  $t_1$ —the upper intersection of discordia age;  $t_2$ —the lower intersection of discordia age.

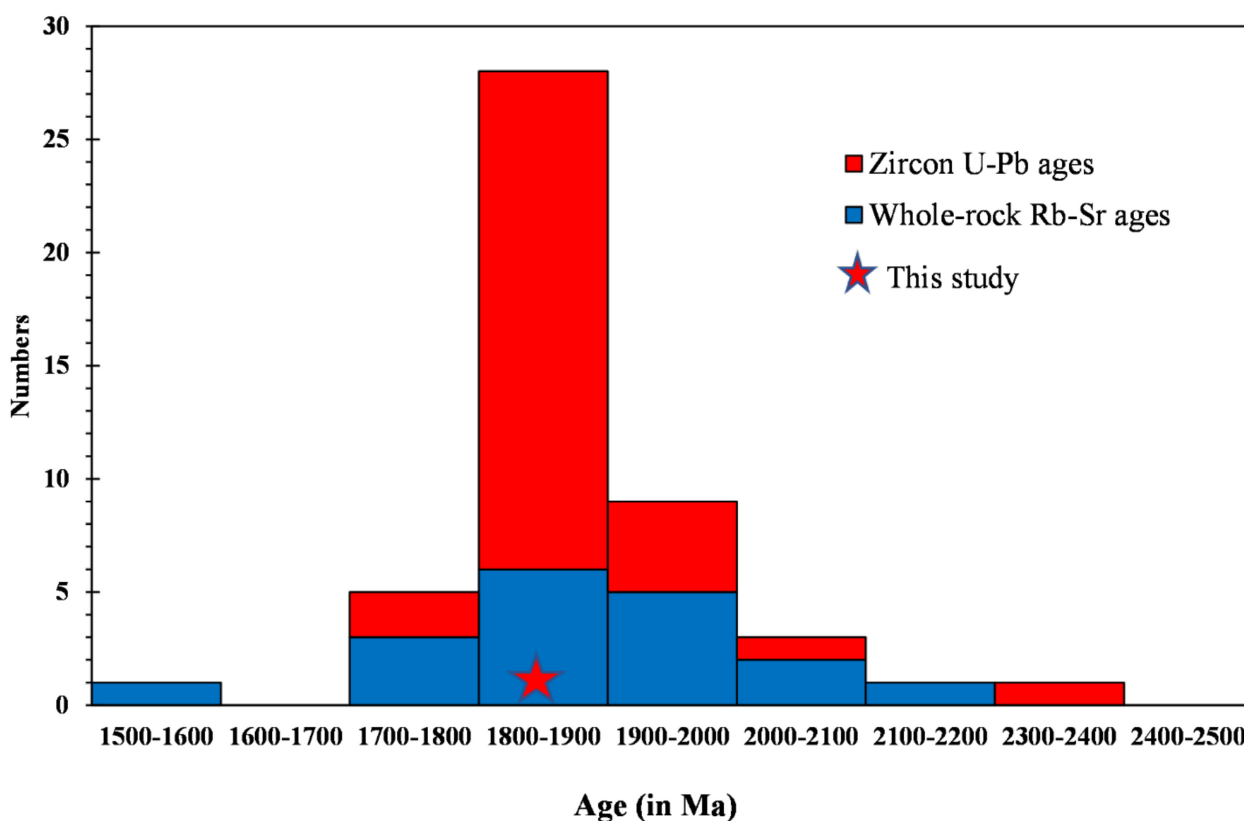


**Figure 11.** Histogram of the published geochronological data set on Paleoproterozoic granites of Lesser Himalayan (Table 3) and age of studied Chail Group granites. (Star: discordant analytical points from both samples form a common isochron with an upper intersection of  $1845 \pm 19$  Ma, Figure 10).

Evidence of old cores in zircons from granites varying in age from 3.5 to 2.1 Ga is analyzed to understand the genesis of the protolith. The scarce old cores of zircons can be divided into three age groups: Paleoproterozoic (3.52 Ga), Neoproterozoic (2.78 Ga and 2.62 Ga), and Paleoproterozoic (2.1 Ga). This diversity suggests that granites originated from sediments formed by the destruction of rocks varying in age from Paleoproterozoic to Paleoproterozoic and supports the notion that these granites are S-type granites [50].

The geochemical characteristics of the zircons suggest that most were produced by magmatic processes. However, the 2.78 Ga grain is depleted in HREE, which is characteristic of garnet-bearing metamorphic rocks [12,51,52]. In the Northern Indian plate, the Aravalli and Bundelkhand Cratons and the Paleoproterozoic Aravalli Fold Belt are recognized [53]. The Bundelkhand Craton contains Paleoproterozoic (3.6–3.2 Ga) granitoids [54–56] and signs of Neoproterozoic (2.78 and 2.69 Ga) eclogite- and amphibolite-facies metamorphism [57–59]. Thus, Bundelkhand Craton rocks could have been the source of Paleoproterozoic magmatic and Archean metamorphic zircons in the granites discussed.

Moreover, Neoproterozoic (2.58–2.5 Ga) granites are widespread in the Bundelkhand and Aravalli Cratons. The Aravalli Craton is known to contain 2.62 Ga Gingla Granite [60,61], which could have been the source of the  $2.62 \pm 0.05$  Ga magmatic zircons in the Himalayan granitoids discussed. The Paleoproterozoic (ca 2.1 Ga) magmatic zircons in these rocks were most probably derived from the  $1.90 \pm 0.08$  Ga Darwal Granite, formed during the Aravalli orogeny [61]. Thus, the 3.5–2.1 Ga cores of zircons from Paleoproterozoic Chail Group granites (Garhwal Lesser Himalayan) could have originated from the Aravalli and Bundelkhand Cratons and the Paleoproterozoic Aravalli Fold Belt. The old block of Indian shield crust comprised the entire western flank of the Columbia Supercontinent in the Paleoproterozoic time (ca. 1.85 Ga) [62]. Here, 1.85 Ga Chail Group granites could have been formed during accretion–collision events.

Collisional granites in orogenic belts are significant because their age can be used to estimate the minimum duration of an orogeny [63–65]. Most Paleoproterozoic granites in LHS (Table 3) are formed in convergent (arc and collisional) environments. For example, Ramgarh gneiss (1765 Ma), Askot granite gneiss (1857 Ma), Chiplakot granite gneiss (1924 Ma), and Lingtse orthogneiss (resembles Ulleri gneiss of Nepal Lesser Himalaya) also formed between 1850 and 1810 Ma.

**Table 3.** Age and geodynamics of Paleoproterozoic granites, Lesser Himalayan Sequences, from northwest to northeast.

Region	Rock Type	Age	Remark
Askot (Kumaun Lesser Himalaya) [65]	Granite gneiss and porphyritic granite gneiss	Ca. 1857 Ma (U–Pb zircon)	Arc-related
Askot (Kumaun Lesser Himalaya) [66]	Augen gneiss	Ca. 1810 Ma (Whole-rock Rb–Sr)	–
Ramgarh (Kumaun Lesser Himalaya) [67]	Granite gneiss	Ca. 1765 Ma (Whole-rock Rb–Sr)	–
Rangit window (Lesser Himalaya of Darjeeling–Sikkim) [68]	Pegmatite	Ca. 1850 Ma (Ar–Ar muscovite)	–
Lingste (MCT zone, Sikkim Himalaya) [69,70]	Ortho gneiss	Ca. 1840 Ma Ca. 1830 Ma (U–Pb zircon)	–
Bomdila (Arunachal Lesser Himalaya) [71–73]	Granite gneiss	Ca. 1743 Ma Ca. 1752 Ma (U–Pb zircon)	Formed by partial melting of metasediments
Shang (Besham, NW Himalaya, Pakistan) [74]	Ortho gneiss	Ca. 1864 Ma (U–Pb zircon)	–
Wangtu (MCT zone, Sutlej valley) [75]	Ortho gneiss	Ca. 1.8 Ga Ma (U–Pb zircon)	–
Jutogh Gr (MCT zone, Sutlej valley) [76]	Leucogranite	Ca. 1810 Ma (U–Pb zircon/uranite)	Formed by crustal melting
Debguru (Kumaun Lesser Himalaya) [77]	Granite gneiss	Ca. 1856 Ma (U–Pb zircon)	–
Along Mandakini River (Kumaun Lesser Himalaya) [77]	Granite gneiss	Ca. 1865 Ma (U–Pb zircon)	–
Amritpur (Kumaun Lesser Himalaya) [78]	Granite	Ca. 1880 Ma (Whole-rock Rb–Sr)	–
Kada and Lhagoi kangari (Tibet Greater Himalayan sequence) [79]	Monzonitic granite gneisses	Ca. 1811 Ma (U–Pb zircon)	–
Ulleri (Nepal Lesser Himalaya) [80]	Ortho gneiss	Ca. 1831 Ma (U–Pb zircon)	–
Daling orthogneiss (Lesser Himalaya of Bhutan) [81]	Ortho gneiss	Ca. 1884 Ma (U–Pb zircon)	–
Salari (Arunachal Lesser Himalaya) [82]	Granite	Ca. 1749 Ma (U–Pb zircon)	Arc-related
Far–Eastern Nepal (Taplejung) [83]	Orthogneiss	1915 ± 15 Ma	Rift-related granitoids
Larji–Kullu–Rampur window (NW Himalaya) [12]	Meta-rhyolite and granite gneiss	Ca. 1.84 Ga (Zircon Pb–Pb evaporation)	Formed by melting of Archean crust
The lesser Himalayan sequence of Nepal Himalaya [13]	Granitic orthogneiss and metavolcanics	Ca. 1780 to 1880 Ma (U–Pb zircon)	Arc-related
Tawaghat (Kumaun Lesser Himalaya) [27]	Granite gneiss	Ca. 1906 Ma (Whole-rock Rb–Sr)	–
Chiplakot (Kumaun Lesser Himalaya) [47]	Granite gneiss	Ca. 1924 Ma (U–Pb zircon)	Arc-related
Munsiari augen gneiss (Kumaun Lesser Himalaya) [47]	Gneisses	Ca. 1955 Ma (U–Pb zircon)	–
Bandal (MCT zone Himachal Himalaya) [48]	Ortho gneiss	Ca. 1860 Ma (U–Pb zircon)	Formed by partial melting of metasediments
Bhatwari (Garhwal Lesser Himalaya) [49]	Gneisses	Ca. 1940 Ma (U–Pb zircon)	Arc-related

Moreover, 1743 Ma [71] and 1752 Ma [72] Ma Bomdila gneiss in Arunachal Pradesh and its equivalent Ziro gneiss in Lower Subansiri are both integral parts of basement-involved imbricated thrusts in the Arunachal Lesser Himalaya [71,73], which are equivalent to the northwest Himachal Himalaya, Garhwal–Kumaun Lesser Himalaya, and Nepal Lesser Himalaya crystalline thrust sheets, which are derived from juvenile and crustal sources in arc-related tectonic settings (Table 3). Any part of Paleoproterozoic granite (for example, Larji-Kullu-Rampur window, NW Himalaya) could be developed in syn- to post-collision environments, as with the studied granites. Leucogranite–pegmatites from the Rangit window, Wangtu (MCT zone, Sutlej valley), Bandal (MCT zone Himachal Himalaya), and Bomdila (Arunachal Lesser Himalaya) are also developed in syn- to post-collision environments (Table 3), as evidenced by three-stage zircon Hf-model ages (2818, 2586–2424, 2393–2250 Ma) [66].

## 7. Conclusions

Zircons from Chail Group granites (Garhwal Lesser Himalayan) display an internal structure typical of magmatic varieties (oscillatory zoning); mineral quartz, apatite, thorite, biotite, allanite, and monazite inclusions; and geochemical characteristics (enrichment in HREE,  $\text{Th}/\text{U} > 0.1$ , and positive  $\text{Ce}/\text{Ce}^*$  and negative  $\text{Eu}/\text{Eu}^*$  anomalies). Hence, these zircons can be regarded as minerals formed at a magmatic stage in the evolution of granites. U–Th–Pb isotope dating of magmatic zircons from two different samples was performed to estimate their age from the upper intersection of the discordia at  $1851 \pm 36$  (MSWD = 2.0,  $n = 15$ ) and  $1839 \pm 38$  (MSWD = 0.94,  $n = 13$ ) Ma, respectively. Combining all of the least discordant analytical points from two samples to form a single isochron line on the U–Pb diagram and age  $1845 \pm 19$  Ma (MSWD = 1.19,  $n = 28$ ) estimate can be regarded as the most adequate.

The cores of three age groups—Paleoarchean (3.52 Ga), Neoproterozoic (2.78 Ga and 2.62 Ga), and Paleoproterozoic (2.1 Ga)—were revealed in zircons from one sample. Zircons aged 3.52, 2.62, and 2.1 Ga are regarded as magmatic based on their geochemical characteristics, and the 2.78 Ga core is metamorphic. Therefore, it can be concluded that these zircons have been derived from Aravalli and Bundelkhand Craton and Paleoproterozoic Aravalli Fold Belt rocks. Studied granites of the Chail Group were formed at 1845 Ma by melting a substrate consisting of rocks varying in age and genesis, which is characteristic of sediments. The discussed Paleoproterozoic granites were formed on the western flank of the Columbia Supercontinent during accretion–collision events.

**Supplementary Materials:** The following are available online at <https://www.mdpi.com/article/10.3390/min11101071/s1>, Figure S1: Various chemical discrimination diagrams for granites of Lesser Garhwal Himalaya. (a) A–C–F diagram [29] Chappell and White 1992). (b)  $\text{Na}_2\text{O}$  versus  $\text{K}_2\text{O}$  diagram [30] (c)  $\text{SiO}_2$  versus  $\text{P}_2\text{O}_5$  diagram [29] (d)  $\text{SiO}_2$  versus  $\text{Na}_2\text{O} + \text{K}_2\text{O}$ – $\text{CaO}$  diagrams (the data for composition fields is from Lachlan Fold Belt) [31], Figure S2: Source discrimination diagram for granites after [32], Figure S3: Primitive mantle-normalized trace elements patterns of the granites [33], Figure S4: Hf–Rb–Ta discrimination diagram [34], Figure S5: Chondrite-normalized [46] REE concentrations in granite TG17-01 and calculated REE concentrations based on zircon/melt partition coefficient for element Grc1 [50] and Grc2 [83], Figure S6: Chondrite-normalized [46] REE concentrations in granite TG17-04 and calculated REE concentrations based on zircon/melt partition coefficient for element Grc1 [50] and Grc2 [83], Table S1: Whole-rock geochemistry of granite samples (major elements in wt. % and trace elements in ppm), Table S2: Calculations of REE and Y in TG17-01 granites, based on data on their concentrations in Paleoproterozoic zircons, Table S3: Calculations of REE and Y concentrations in TG17-04 Granites, based on data on their concentrations in Paleoproterozoic zircons, Table S4: Average content (610av, 612av, 614av) and standard deviation (SD) of trace elements in reference materials NIST SRM 610, 612, 614 (#610, #612, #614) during measurements. The accepted maintenance of trace elements in reference materials #610, #612, #614 on [42].

**Author Contributions:** Conceptualization, S.M. and A.I.S.; methodology, A.I.S., A.V.K. and N.S.N.; validation, S.M., A.I.S., S.A.S. and N.S.N.; investigation, S.M.; resources, A.I.S. and S.A.S.; data curation, A.I.S. and A.V.K.; writing—original draft preparation, S.M.; writing—review and editing, A.I.S., S.A.S., A.V.K. and N.S.N.; visualization, S.M. and A.I.S.; supervision, A.I.S. and S.A.S.; project administration, S.M. and A.I.S.; funding acquisition, S.A.S. and A.I.S. All authors have read and agreed to the published version of the manuscript.

**Funding:** This research was funded by state assignment to the Institute of Geology Karelian Research Centre RAS AAAA-A18-118020290085-4.

**Data Availability Statement:** Not applicable.

**Acknowledgments:** We thank H.C. Nainwal (Department of Geology, HNBGU, Srinagar) for the continuous encouragement and for providing infrastructural facilities to S.M. S.M. acknowledges the DST-INSPIRE fellowship (IF160096). This paper is part of the doctoral research of S.M. and the contribution of A.I.S., A.K., S.A.S. and N.S.N. to the KarRC R.A.S. project A18-118020290085. We thank Xiaoli Li and F. Ma, Peking University, Beijing, China, for their help in the dating of zircons and the determination of their geochemistry. We are thankful to Saurabh Gupta (Nainital) for the revision of the manuscript. Critical and constructive comments from three anonymous reviewers helped to improve the presentation and clarify the authors' meaning.

**Conflicts of Interest:** The authors declare no conflict of interest.

## Appendix A

### *Whole-Rock Geochemistry*

Whole-rock geochemical analysis of samples was carried out at the Centre for Collective Usage, Karelian Research Centre, R.A.S. (Petrozavodsk, Russia). To determine the concentrations of the rock-forming elements, sample powder was melted and then treated with Na<sub>2</sub>CO<sub>3</sub> (sodium bicarbonate). The solution was then leached with dilute HCl (hydrochloric acid) to determine the element concentrations. The gravimetric method was used to determine the SiO<sub>2</sub> concentration in the resulting solution after it was precipitated with gelatin for the first time (with absorption photometry, PerkinElmer, and by X-ray fluorescence (XRF) using spectrometry ARL ADVAN X). The concentrations of Mg, Ca, Al, and Fe was determined using a sophisticated metric calculation. The precision of the major and trace element concentrations of the samples were determined using examinations of the standard samples GSP-2 (Granodiorite, Silver Plume, Colorado) and BHVO-2 (Basalt, Hawaiian Volcanic Observatory) (Supplementary Table S1) [84].

In contrast, the concentrations of Ti and P were obtained photometrically. Two parallel estimations were added to ensure that the calculation accuracy remained within an acceptable range of error. For Si, the accuracy was within 0.7 percent; for Fe, Al, Ca, and Mg, it was within 0.5 percent; and for P and Ti, it was within 0.3 percent. The amounts of trace elements in the samples were determined using an X Series-2 inductively coupled plasma mass spectrometer (ICP-MS) (Thermo Fisher Scientific, Waltham, MA, USA). Svetov et al. [85] and Singh and Slabunov [86] outline the approach and methods used in this investigation in detail. The samples were degraded in an autoclave using acid dissolution. For analysis, weighted sections of material weighing 0.1 g were employed. The substances studied were decomposed in conjunction with two standard samples and two reference samples (blank samples) (GSP-2 and BHVO-2).

## References

1. Hoskin, P.W.O.; Schaltegger, U. The composition of zircon and igneous and metamorphic petrogenesis. *Rev. Mineral. Geochem.* **2003**, *53*, 27–62. [[CrossRef](#)]
2. Sawka, W.N. REE and trace element variations in accessory minerals and hornblende from the strongly zoned McMurry Meadows Pluton, California. *Earth Environ. Sci. Trans. R. Soc. Edinb.* **1988**, *79*, 157–168.
3. Bea, F. Residence of REE, Y, Th and U in granites and crustal protoliths; implications for the chemistry of crustal melts. *J. Petrol.* **1996**, *37*, 521–552. [[CrossRef](#)]
4. O'Hara, M.J.; Fry, A.; Prichard, H.M. Minor phases as Carriers of trace elements in non-modal crystal-liquid separation processes I: Basic relationships. *J. Petrol.* **2001**, *42*, 1869–1886. [[CrossRef](#)]

5. Belousova, E.A.; Griffin, W.L.; O'Reilly, S.Y.; Fisher, N.I. Igneous zircon: Trace element composition as an indicator of source rock type. *Contrib. Mineral. Petrol.* **2002**, *143*, 602–622. [[CrossRef](#)]
6. Fedotova, A.A.; Bibikova, E.V.; Simakin, S.G. Ion-microprobe zircon geochemistry as an indicator of mineral genesis during geochronological studies. *Geochem. Int.* **2008**, *46*, 912–927. [[CrossRef](#)]
7. Wu, Y.; Zheng, Y. Genesis of zircon and its constraints on interpretation of U-Pb age. *Chinese Sci. Bull.* **2004**, *49*, 1554–1569. [[CrossRef](#)]
8. Singh, S. Himalayan Magmatism through space and time. *Episodes* **2020**, *43*, 358–368. [[CrossRef](#)]
9. Sandeep, S. Status of magmatic ages in the Himalaya: A review of geochronological studies. *J. Indian Geophys. Union* **2001**, *5*, 57–72.
10. Parrish, R.R.; Hodges, V. Isotopic constraints on the age and provenance of the Lesser and Greater Himalayan sequences, Nepalese Himalaya. *Geol. Soc. Am. Bull.* **1996**, *108*, 904–911. [[CrossRef](#)]
11. Miller, C.; Klötzli, U.; Frank, W.; Thöni, M.; Grasemann, B. Proterozoic crustal evolution in the N.W. Himalaya (India) as recorded by circa 1.80 Ga mafic and 1.84 Ga granitic magmatism. *Precambrian Res.* **2000**, *103*, 191–206. [[CrossRef](#)]
12. Kohn, M.J.; Paul, S.K.; Corrie, S.L. The lower Lesser Himalayan sequence: A Paleoproterozoic arc on the northern margin of the Indian plate. *Geol. Soc. Am. Bull.* **2010**, *122*, 323–335. [[CrossRef](#)]
13. Larson, K.; Cottle, J.; Lederer, G.; Rai, S.M. Defining shear zone boundaries using fabric intensity gradients: An example from the east-central Nepal Himalaya. *Geosphere* **2017**, *13*, 771–781. [[CrossRef](#)]
14. Jain, A.K.; Banerjee, D.M.; Kale, V.S. *Tectonics of the Indian Subcontinent: An Introduction*; Springer: Cham, Switzerland, 2020; ISBN 9783030428440.
15. Medlicott, H.B.; Blanford, W.T.; Ball, V.; Mallett, F.R. *A Manual of the Geology of India: Peninsular Area*; Medlicott, H.B., Blanford, H.B., Eds.; Geological Survey of India: New Delhi, India, 1879.
16. Heim, A.; Gansser, A. *Central Himalaya: Geological Observations of the Swiss Expedition*; Hindustan Publishing Corporation: Delhi, India, 1936; Volume 73.
17. Thakur, V.C. Active tectonics of Himalayan Frontal Fault system. *Int. J. Earth Sci.* **2013**, *102*, 1791–1810. [[CrossRef](#)]
18. Valdiya, K.S. The two intracrustal boundary thrusts of the Himalaya. *Tectonophysics* **1980**, *66*, 323–348. [[CrossRef](#)]
19. Metcalfe, R.P. Pressure, temperature and time constraints on metamorphism across the Main Central Thrust zone and High Himalayan Slab in the Garhwal Himalaya. *Geol. Soc. Spec. Publ.* **1993**, *74*, 485–509. [[CrossRef](#)]
20. Stephenson, B.J.; Waters, D.J.; Searle, M.P. Inverted metamorphism and the Main Central Thrust: Field relations and thermobarometric constraints from the Kishtwar Window, NW Indian Himalaya. *J. Metamorph. Geol.* **2000**, *18*, 571–590. [[CrossRef](#)]
21. Thakur, V.C. Geology of western Himalaya. *Phys. Chem. Earth* **1992**, *19*, 1–355.
22. Negi, S.S.; Sinha, A.K.; Pandey, B.K. A preliminary report on the geology and structure of the Rudraprayag-Tilwara-Mayali area of Garhwal Himalaya. *Himalayan Geol.* **1980**, *10*, 211–219.
23. Saklani, P.S.; Nainwal, D.C.; Singh, V.K. Geometry of the composite Main Central Thrust (MCT) in the Yamuna Valley, Garhwal Himalaya, India. *Neues Jahrb. Für Geol. Paläontol. Monatsh.* **1991**, *6*, 364–380. [[CrossRef](#)]
24. Saklani, P.S. *Geology of the Lower Himalaya (Garhwal)*; International Books and Periodicals Supply Service: New Delhi, India, 1996; p. 246.
25. Ahmad, T.; Mukherjee, P.K.; Trivedi, J.R. Geochemistry of Precambrian mafic magmatic rocks of the Western Himalaya, India: Petrogenetic and tectonic implications. *Chem. Geol.* **1999**, *160*, 103–119. [[CrossRef](#)]
26. Singh, V.P.; Bhanot, V.B.; Singh, R.P. Geochronology of the granitic and gneissic rocks from Munsiri, Namik and Tawaghat areas of the Central Crystalline Zone, Kumaun Himalaya, UP. In *Preprint Presented at the 3rd National Symposium on Mass Spectrometry, Hyderabad, India, 22–24 September 1985*; The Geological Society: Hyderabad, India, 1985; pp. 22–24.
27. Raju, B.N.V.; Chabria, T.; Prasad, R.N.; Mahadevan, T.M.; Bhalla, N.S. Early Proterozoic Rb–Sr isochron age for Central Crystalline, Bhilangana valley, Garhwal Himalaya. *Himalayan Geol.* **1982**, *12*, 196–205.
28. Kretz, R. Symbols for rock-forming minerals. *Am. Mineral.* **1983**, *68*, 277–279.
29. Chappell, B.W.; White, A.J.R. I- and S-type granites in the Lachlan Fold Belt. *Earth Environ. Sci. Trans. R. Soc. Edinburgh.* **1992**, *83*, 1–26. [[CrossRef](#)]
30. Chappell, B.W.; White, A.J. Two contrasting granite types: 25 years later. *Aust. J. Earth Sci.* **2001**, *48*, 489–499. [[CrossRef](#)]
31. Frost, B.R.; Barnes, C.G.; Collins, W.J.; Arculus, R.J.; Ellis, D.J.; Frost, C.D. A geochemical classification for granitic rocks. *J. Petrol.* **2001**, *42*, 2033–2048. [[CrossRef](#)]
32. Laurent, O.; Martin, H.; Moyen, J.F.; Doucelance, R. The diversity and evolution of late-Archean granitoids: Evidence for the onset of “modern-style” plate tectonics between 3.0 and 2.5 Ga. *Lithos* **2014**, *205*, 208–235. [[CrossRef](#)]
33. McDonough, W.F.; Sun, S.S. The composition of the Earth. *Chem. Geol.* **1995**, *120*, 223–253. [[CrossRef](#)]
34. Harris, N.B.; Pearce, J.A.; Tindle, A.G. Geochemical characteristics of collision-zone magmatism. *Geol. Soc. Spec. Publ.* **1986**, *19*, 67–81. [[CrossRef](#)]
35. Mukherjee, P.K.; Singhal, S.; Adlakha, V.; Rai, S.K.; Dutt, S.; Kharya, A.; Gupta, A.K. In situ U-Pb zircon micro-geochronology of MCT zone rocks in the Lesser Himalaya using LA-MC-ICPMS technique. *Curr. Sci.* **2017**, *112*, 802–810. [[CrossRef](#)]
36. Chahal, P.; Kumar, A.; Sharma, C.P.; Singhal, S.; Sundriyal, Y.P.; Srivastava, P. Late Pleistocene history of aggradation and incision, provenance and channel connectivity of the Zanskar River, NW Himalaya. *Glob. Planet. Chang.* **2019**, *178*, 110–128. [[CrossRef](#)]

37. Zaitceva, M.V.; Pupyshv, A.A.; Shchapova, J.V.; Votyakov, S.L. Methodological aspects of U/Pb dating of zircons using multicollector mass spectrometer with inductively coupled plasma NEPTUNE PLUS with NWR 213 attachment for laser ablation. *Anal. Control.* **2016**, *20*, 121–137. [[CrossRef](#)]
38. Wiedenbeck, M.A.; Alle, P.; Corfu, F.; Griffin, W.L.; Meier, M.; Oberli, F.V.; Quadt, A.V.; Roddick, J.C.; Spiegel, W. Three natural zircon standards for U-Th-Pb, Lu-Hf, trace element and REE analyses. *Geostand. Newsl.* **1995**, *19*, 1–23. [[CrossRef](#)]
39. Sláma, J.; Košler, J.; Condon, D.J.; Crowley, J.L.; Gerdes, A.; Hanchar, J.M.; Horstwood, M.S.A.; Morris, G.A.; Nasdala, L.; Norberg, N.; et al. Plešovice zircon—A new natural reference material for U-Pb and Hf isotopic microanalysis. *Chem. Geol.* **2008**, *249*, 1–35. [[CrossRef](#)]
40. Andersen, T. Correction of common lead in U-Pb analyses that do not report  $^{204}\text{Pb}$ . *Chem. Geol.* **2002**, *192*, 59–79. [[CrossRef](#)]
41. Ludwig, K.R. Eliminating mass-fractionation effects on U-Pb isochron ages without double spiking. *Geochim. Cosmochim. Acta* **2001**, *65*, 3139–3145. [[CrossRef](#)]
42. Jochum, K.P.; Stoll, B. Reference materials for elemental and isotopic analysis. In *LA-ICP-MS in the Earth Sciences: Current Practices and Outstanding Issues*; Sylvester, P., Ed.; Mineralogical Association of Canada: Québec, QC, USA, 2008; Volume 40, pp. 320–326.
43. Wetherill, G.W. Discordant uranium-lead ages. *Trans. Amer. Geophys. Union* **1956**, *37*, 320–326. [[CrossRef](#)]
44. Sawyer, E.W.; Cesare, B.; Brown, M. When the Continental Crust Melts. *Elements* **2011**, *17*, 229–234. [[CrossRef](#)]
45. Watson, E.B.; Wark, D.A.; Thomas, J.B. Crystallization thermometers for zircon and rutile. *Contrib. Mineral. Petrol.* **2006**, *151*, 413–433. [[CrossRef](#)]
46. Nakamura, N. Determination of REE, Ba, Fe, Mg, Na and K in carbonaceous and ordinary chondrites. *Geochimic. Cosmochim. Acta* **1974**, *38*, 757–775. [[CrossRef](#)]
47. Sen, A.; Sen, K.; Srivastava, H.B.; Singhal, S.; Phukon, P. Age and geochemistry of the Paleoproterozoic Bhatwari Gneiss of Garhwal Lesser Himalaya, NW India: Implications for the pre-Himalayan magmatic history of the Lesser Himalayan basement rocks. *Geol. Soc. Spec. Publ.* **2019**, *481*, 319–339. [[CrossRef](#)]
48. Singh, S.; Jain, A.K.; Barley, M.E. SHRIMP U-Pb c. 1860 Ma anorogenic magmatic signatures from the N.W. Himalaya: Implications for Paleoproterozoic assembly of the Columbia supercontinent. *Geol. Soc. Spec. Publ.* **2009**, *323*, 283–300. [[CrossRef](#)]
49. Phukon, P.; Sen, K.; Srivastava, H.B.; Singhal, S.; Sen, A. U-Pb geochronology and geochemistry from the Kumaun Himalaya, NW India, reveal Paleoproterozoic arc magmatism related to formation of the Columbia supercontinent. *Bull. Geol. Soc. Am.* **2018**, *130*, 1164–1176. [[CrossRef](#)]
50. Mishra, S.; Singh, V.K.; Slabunov, A.I.; Nainwal, H.C.; Singh, P.K.; Chaudhary, N.; Nainwal, D.C. Geochemistry and geodynamic setting of Paleoproterozoic granites of Lesser Garhwal Himalaya, India. *J. Geosci. Eng. Environ. Technol.* **2019**, *25*, 28–38. [[CrossRef](#)]
51. Rubatto, D.; Hermann, J. Experimental zircon/melt and zircon/garnet trace element partitioning and implications for the geochronology of crustal rocks. *Chem. Geol.* **2007**, *241*, 38–61. [[CrossRef](#)]
52. Rubatto, D. Zircon trace element geochemistry: Partitioning with garnet and the link between U-Pb ages and metamorphism. *Chem. Geol.* **2002**, *184*, 123–138. [[CrossRef](#)]
53. Ramakrishnan, M.; Vaidyanadhan, R. *Geology of India*; Geological Society of India: Bangalore, India, 2010; Volume 2.
54. Mondal, M.E.A.; Goswami, J.N.; Deomurari, M.P.; Sharma, K.K. Ion microprobe  $^{207}\text{Pb}/^{206}\text{Pb}$  ages of zircons from the Bundelkhand massif, northern India: Implications for crustal evolution of the Bundelkhand-Aravalli protocontinent. *Precambrian Res.* **2002**, *117*, 85–100. [[CrossRef](#)]
55. Kaur, P.; Zeh, A.; Chaudhri, N. Characterization and U-Pb-Hf isotope record of the 3.55Ga felsic crust from the Bundelkhand Craton, northern India. *Precambrian Res.* **2014**, *255*, 236–244. [[CrossRef](#)]
56. Saha, L.; Frei, D.; Gerdes, A.; Pati, J.K.; Sarkar, S.; Patole, V.; Bhandari, A.; Nasipuri, P. Crustal geodynamics from the Archaean Bundelkhand Craton, India: Constraints from zircon U-Pb-Hf isotope studies. *Geol. Mag.* **2016**, *153*, 79–192. [[CrossRef](#)]
57. Saha, L.; Pant, N.C.; Pati, J.K.; Upadhyay, D.; Berndt, J.; Bhattacharya, A.; Satynarayanan, M. Neoproterozoic high-pressure margarite-phengitic muscovite-chlorite corona mantled corundum in quartz-free high-Mg, Al phlogopite-chlorite schists from the Bundelkhand craton, north central India. *Contrib. Mineral. Petrol.* **2011**, *161*, 511–530. [[CrossRef](#)]
58. Slabunov, A.I.; Singh, V.K. Meso–Neoproterozoic crustal evolution of the Bundelkhand Craton, Indian Shield: New data from greenstone belts. *Int. Geol. Rev.* **2019**, *61*, 1409–1428. [[CrossRef](#)]
59. Sibelev, O.S.; Slabunov, A.I.; Mishra, S.; Singh, V.K. Metamorphism of the Central Bundelkhand Greenstone Complex, Indian Shield: Mineral Compositions, Paragenesis's, and P–T Path. *Petrology* **2021**, *29*, 404–438. [[CrossRef](#)]
60. Kaur, P.; Zeh, A.; Chaudhri, N. Archean crustal evolution of the Aravalli Banded Gneissic Complex, NW India: Constraints from zircon U-Pb ages, Lu-Hf isotope systematics, and whole-rock geochemistry of granitoids. *Precambrian Res.* **2019**, *327*, 81–102. [[CrossRef](#)]
61. Roy, A.B.; Purohit, R. *Concept of Indian Shield: Evolution and Reconstitution*; Elsevier: Amsterdam, Netherlands, 2018; ISBN 9780128098394.
62. Hou, G.; Santosh, M.; Qian, X.; Lister, G.S.; Li, J. Configuration of the Late Paleoproterozoic supercontinent Columbia: Insights from radiating mafic dyke swarms. *Gondwana Res.* **2008**, *14*, 395–409. [[CrossRef](#)]
63. Witt, D.; Davy, R. Geology and geochemistry of Archaean granites in the Kalgoorlie region of the Eastern Goldfields, Western Australia: A syn-collisional tectonic setting? *Precamb. Res.* **1997**, *83*, 133–183. [[CrossRef](#)]
64. Harrison, T.M.; Grove, M.; McKeegan, K.D.; Coath, C.D.; Lovera, O.M.; Le Fort, P. Origin and episodic emplacement of the Manaslu intrusive complex, Central Himalaya. *J. Petrol.* **1999**, *40*, 3–19. [[CrossRef](#)]

65. Johnson, S.; Poujol, M.; Kisters, A.F.M. Constraining the timing and migration of collisional tectonics in the Damara Belt, Namibia: U–Pb zircon ages for the syntectonic Salem-type Stink bank granite. *S. Afr. J. Geol.* **2006**, *109*, 611–624. [[CrossRef](#)]
66. Mandal, S.; Robinson, D.M.; Kohn, M.J.; Khanal, S.; Das, O.; Bose, S. Zircon U–Pb ages and Hf isotopes of the Askot klippe, Kumaun, northwest India: Implications for Paleoproterozoic tectonics, basin evolution and associated metallogeny of the northern Indian cratonic margin. *Tectonics* **2016**, *35*, 965–982. [[CrossRef](#)]
67. Kumar, S.; Rino, V. Mineralogy and geochemistry of microgranular enclaves in Paleoproterozoic Malanjhand granitoids, central India: Evidence of magma mixing, mingling, and chemical equilibration. *Contrib. Mineral. Petrol.* **2006**, *152*, 591–609. [[CrossRef](#)]
68. Trivedi, J.R.; Gopalan, K.; Valdiya, K.S. Rb–Sr ages of granitic rocks within the Lesser Himalayan Nappes, Kumaun, India. *J. Geol. Soc. India* **1984**, *25*, 641–654.
69. Acharyya, S.K.; Ghosh, S.; Mandal, N.; Bose, B.; Kanchan, P. Pre-Himalayan tectono-magmatic imprints in the Darjeeling–Sikkim Himalaya (D.S.H.) constrained by  $^{40}\text{Ar}/^{39}\text{Ar}$  dating of muscovite. *J. Asian Earth Sci.* **2017**, *146*, 211–220. [[CrossRef](#)]
70. Mottram, C.M.; Argles, T.W.; Harris, N.B.W.; Parrish, R.R.; Horstwood, M.S.A.; Warren, C.J.; Gupta, S. Tectonic interleaving along the Main Central Thrust, Sikkim Himalaya. *J. Geol. Soc.* **2014**, *171*, 255–268. [[CrossRef](#)]
71. Yin, A.; Dubey, C.S.; Webb, A.A.G.; Kelty, T.K.; Grove, M.; Gehrels, G.E.; Burgess, W.P. Geologic correlation of the Himalayan orogen and Indian craton: Part 1. Structural geology, U–Pb zircon geochronology, and tectonic evolution of the Shillong Plateau and its neighbouring regions in NE India. *Geol. Soc. Am. Bull.* **2010**, *122*, 336–359. [[CrossRef](#)]
72. Pathak, M.; Kumar, S. Petrology, geochemistry and zircon U–Pb–Lu–Hf isotopes of Paleoproterozoic granite gneiss from Bomdila in the western Arunachal Himalaya, NE India. *Geol. Soc. Spec. Publ.* **2019**, *481*, 341–377. [[CrossRef](#)]
73. Goswami, S.A.; Bhowmik, S.K.; Dasgupta, S. Petrology of a non-classical Barrovian inverted metamorphic sequence from the western Arunachal Himalaya, India. *J. Asian Earth Sci.* **2009**, *36*, 390–406. [[CrossRef](#)]
74. DiPietro, J.A.; Isachsen, C.E. U–Pb zircon ages from the Indian plate in northwest Pakistan and their significance to Himalayan and pre-Himalayan geologic history. *Tectonics* **2001**, *20*, 510–525. [[CrossRef](#)]
75. Richards, A.; Argles, T.; Harris, N.; Parrish, R.; Ahmad, T.; Darbyshire, F.; Draganits, E. Himalayan architecture constrained by isotopic tracers from clastic sediments. *Earth Planet. Sci. Lett.* **2005**, *236*, 773–796. [[CrossRef](#)]
76. Chambers, J.A.; Argles, T.W.; Horstwood, M.S.A.; Harris, N.B.W.; Parrish, R.R.; Ahmad, T. Tectonic implications of Palaeoproterozoic anatexis and Late Miocene metamorphism in the Lesser Himalayan sequence, Sutlej Valley, NW India. *J. Geol. Soc.* **2008**, *165*, 725–737. [[CrossRef](#)]
77. Cs el erier, J.; Harrison, T.M.; Webb, A.A.G.; Yin, A. The Kumaun and Garwhal Lesser Himalaya, India: Part 1. Structure and stratigraphy. *Geol. Soc. Am. Bull.* **2009**, *121*, 1262–1280. [[CrossRef](#)]
78. Varadarajan, S. Potassium argon ages of the Amritpur Granite, dist. Nainital, Kumaun Himalaya and its stratigraphic position. *J. Geol. Soc. India* **1978**, *19*, 380–381.
79. Liao, Q.; Li, D.; Lu, L.; Yuan, Y.M.; Chu, L.L. Paleoproterozoic granitic gneisses of the Dinggye and Lhagoi Kangri areas from the higher and northern Himalaya, Tibet: Geochronology and implications. *Sci. China Ser. D-Earth Sci.* **2008**, *51*, 240. [[CrossRef](#)]
80. DeCelles, P.G.; Gehrels, G.E.; Quade, J.; LaReau, B.; Spurlin, M. Tectonic implications of U–Pb zircon ages of the Himalayan orogenic belt in Nepal. *Science* **2000**, *288*, 497–499. [[CrossRef](#)]
81. Long, S.; McQuarrie, N.; Tobgay, T.; Grujic, D. Geometry and crustal shortening of the Himalayan fold-thrust belt, eastern and central Bhutan. *Geol. Soc. Am. Bull.* **2011**, *123*, 1427–1447. [[CrossRef](#)]
82. Pathak, M. Mineralogy and Geochemistry of Felsic Magmatic Rocks in the Kameng District, Western Arunachal Himalaya. Ph.D. Thesis, Kumaun University, Nainital, India, 2012. unpublished.
83. Imayama, T.; Arita, K.; Fukuyama, M.; Yi, K.; Kawabata, R. 1.74 Ga crustal melting after rifting at the northern Indian margin: Investigation of mylonitic orthogneisses in the Kathmandu area, central Nepal. *Int. Geol. Rev.* **2019**, *61*, 1207–1221. [[CrossRef](#)]
84. Wilson, S.A. *Data Compilation for USGS Reference Material GSP-2, Granodiorite, Silver Plume, Colorado*; US Geological Survey Open-File Report; US Geological Survey: Denver, CO, USA, 1998; pp. 11–12.
85. Svetov, S.A.; Stepanova, A.V.; Chazhengina, S.Y.; Svetova, E.N.; Rybnikova, Z.P.; Mikhailova, A.I.; Paramonov, A.S.; Utitsyna, V.L.; Ekhova, M.V.; Kolodey, B.S. Precision geochemical (ICP-MS, LA-ICP-MS) analysis of rock and mineral composition: The method and accuracy estimation in the case study of Early Precambrian mafic complexes. *Trans. Karelian Res. Cent. Russ. Acad. Sci.* **2015**, *7*, 54–73.
86. Singh, V.K.; Slabunov, A. The Central Bundelkhand Archaean greenstone complex, Bundelkhand craton, central India: Geology, composition, and geochronology of supracrustal rocks. *Int. Geol. Rev.* **2015**, *57*, 1349–1364. [[CrossRef](#)]